

THE GLOBAL AND RADIAL STELLAR MASS ASSEMBLY OF MILKY WAY-SIZED GALAXIES

VLADIMIR AVILA-REESE,¹ ALEJANDRO GONZÁLEZ-SAMANIEGO,^{2,3} PEDRO COLÍN,^{3,*} HÉCTOR IBARRA-MEDEL,¹ AND ALDO RODRÍGUEZ-PUEBLA¹

¹*Instituto de Astronomía, Universidad Nacional Autónoma de México, A.P. 70-264, 04510 CDMX, México*

²*Center for Cosmology, Department of Physics and Astronomy, University of California at Irvine, Irvine, CA 92697, USA*

³*Instituto de Radioastronomía y Astrofísica, Universidad Nacional Autónoma de México, A.P. 72-3 (Xangari), Morelia, Michoacán 58089, México*

Submitted to ApJ

ABSTRACT

We study the global and radial stellar mass assembly of eight zoomed-in MW-sized galaxies produced in Hydrodynamics cosmological simulations. The disk-dominated galaxies (4) show a fast initial stellar mass growth in the innermost parts, driven mostly by in-situ SF, but since $z \sim 2 - 1$ the SF enters in a long-term quenching phase. The outer regions follow this trend but more gentle as more external they are. As the result, the radial stellar mass growth is highly inside-out due to both the inside-out structural growth and inside-out SF quenching. The half-mass radius evolves fast; for instance, $R_{0.5}(z = 1) < 0.5R_{0.5}(z = 0)$. Two other runs resemble lenticular galaxies. One shows also a pronounced inside-out growth and the other one presents a nearly uniform radial mass assembly. The other two galaxies suffered late major mergers. Their normalized radial mass growth histories (MGHs) are nearly close among them but with periods of outside-in assembly during or after the mergers. For all the simulations, the archaeological radial MGHs calculated from the $z = 0$ stellar-particles age distribution are similar to the current MGHs, which evidences that the mass assembly by ex-situ stars and the radial mass transport do not change significantly their radial mass distributions. Our results agree qualitatively with observational inferences from the fossil record method applied to a survey of local galaxies and from look-back observations of progenitors of MW-sized galaxies. However, the inside-out growth mode is more pronounced and the $R_{0.5}$ growth is faster in simulations than in observational inferences.

Keywords: Galaxies: evolution — Galaxies: formation — Galaxies: kinematics and dynamics — Methods: numerical

1. INTRODUCTION

According to the Λ Cold Dark Matter (Λ CDM) scenario, galaxies form from gas that cools and falls into the central regions of hierarchically growing CDM halos (White & Rees 1978). These halos acquire angular momentum mainly by tidal torques during the linear regime of the perturbation (Peebles 1969; White 1984). The gas infall rate and consequent star formation rate (SFR) in galaxies are expected to be linked to the cosmological dark halo mass accretion rate (e.g., White & Frenk 1991; van den Bosch 2002; Faucher-Giguère, Kereš & Ma 2011; Lilly et al. 2013; Rodríguez-Puebla et al. 2016). Within this scenario, the generic outcome of galaxy formation, under the assumption of gas angular momentum conservation, are disks that assemble their structure inside out (e.g., Larson 1976; Fall & Efstathiou 1980; Gunn 1982; Silk 1987; Mo, Mao & White 1998; Avila-Reese, Firmani & Hernández 1998; Bouwens & Silk 2002; Somerville et al. 2008).

The gas in the inside-out growing disks is transformed gradually into stars. As the result, exponential disks that follow the main observed correlations of disk galaxies and that present negative radial age and color gradients are produced (e.g., Boissier & Prantzos 2000; van den Bosch 2000; Avila-Reese & Firmani 2000; Firmani & Avila-Reese 2000; Stringer & Benson 2007; Dutton 2009, see for a review and more references Mo, van den Bosch & White 2010). The radial stellar and color distributions so established can be further affected by other accretion channels, like infall from filaments (Dekel & Birnboim 2006) or minor mergers (e.g., Barnes & Hernquist 1996; Di Teodoro & Fraternali 2014), by radial gas flows within the disk (e.g., Athanassoula 2003; Pezzulli & Fraternali 2016), and stellar mass re-distribution by internal dynamics processes (e.g., Debattista et al. 2006; Roškar et al. 2008; El-Badry et al. 2016; Berrier & Sellwood 2016). The radial flows play also a role in changing the metallicity radial distribution (e.g., Bilitewski & Schönrich 2012).

On the other hand, the formation of spheroids (elliptical galaxies and bulges) is believed to occur from the morphological transformation of disks, by mergers and internal dynamical processes (see for recent reviews Brooks & Christensen 2016; Kormendy 2016) or infall of gas with misaligned angular momentum (e.g., Scannapieco et al. 2009; Aumer, White & Naab 2014). What does happen with the radial stellar population distribution of spheroids? During early gas-rich mergers, strong bursts of SF are expected to happen across the whole galaxy, but with higher intensity in the center due to gas dissipation and inflow. Late dry mergers as well as internal dynamical processes produce gas infall to the

center but also significant radial mixing of stars. Moreover, spheroid-dominated galaxies across their evolution may suffer one or more phases of disk destruction and rebuilding. All these processes involve active mixing of populations, so they contribute to produce flatter gradients.

The radial distribution of stellar populations can be also affected by processes that abruptly slow down the SFR, particularly in massive galaxies. This rapid shut-off process of SFR is distinctive from the SF histories in the star-forming stage of galaxies, and is often referred as *quenching* (e.g., Faber et al. 2007; Martin et al. 2007; Peng et al. 2010). Diverse mechanisms were proposed to explain the global quenching of galaxies (for reviews, see e.g., Kormendy 2016; Smethurst et al. 2017) but less is known about the spatial behavior of quenching. According to some theoretical models, the quenching happens in the central regions and/or start there and then extend to the outer ones, that is, the quenching is the inside out. This could be the case for the quenching due to negative feedback of an Active Galactic Nucleus (AGN), and due to the formation of stellar spheroids/bulges that stabilize the gas in the galactic disk, suppressing the SF efficiency (Elmegreen, Bournaud & Elmegreen 2008; Martig et al. 2009) or due to the presence of bars that funnel gas to the center, where gas is exhausted by SF (Sheth et al. 2005). The last two processes are known as “morphological” quenching. More recently, Dekel & Burkert (2014, see also Tacchella et al. 2016b) have proposed a quenching process, based on the dissipative shrinkage of the high-redshift gaseous disk, the triggering of intense SF in the dense centre (blue nugget phase), and the consequent rapid gas consumption and outflows that produce an inside-out quenching.

Both the structural inside-out growth of galaxies and the inside-out SF quenching imply that the inner stellar populations result older than the outer ones and that the stellar half-mass radius grows with time. An open question is which of these processes dominates in the evolution of galaxies and what signatures evidence the dominion of one or another of these processes (Lian et al. 2017).

1.1. Cosmological numerical simulations

As discussed above, the way galaxies establish their radial stellar population and mass distributions is complex (see also Pezzulli & Fraternali 2016). The involved processes are: (1) the structural build-up from cold gas accreted from the cosmic dark matter web, (2) the in-situ SF and its eventual quenching across the galaxy, (3) the mass and angular momentum radial transport that gas/stars may suffer, and (4) the accretion of ex-

situ stars and gas in mergers. In principle, all this complexity, which implies non-linear gravitational evolution, baryonic physics, galaxy dynamical processes, etc., can be followed in the N-body + Hydrodynamics cosmological simulations, though it is important to bear in mind that the spatial resolution limits the ability to follow several of the multi-scale physical and dynamical processes of galaxy evolution. Most of previous numerical works have focused on the evolution of global galaxy properties. There are only a few works that present a detailed study of the radial evolution of galaxies down to $z = 0$ (e.g., Bird et al. 2013; Aumer, White & Naab 2014; Grand et al. 2017) or at high redshifts (e.g., Zolotov et al. 2015; Tacchella et al. 2016a,b). Time is ripe to study in more detail the spatially-resolved evolution of simulated galaxies given that observations provide now valuable information on that, for instance, on the SF and stellar mass growth histories (MGHs) as a function of radius for galaxies from large surveys (see below).

The main goal of the present paper is namely to study the radial stellar mass assembly and the establishment of the stellar age distribution along the radius of a suite of eight simulated 'field' Milky Way(MW)-sized galaxies presented in Colín et al. (2016). The simulations do not suffer the overcooling and angular momentum catastrophe problems due to an adequate SF/feedback implementation (see for a related discussion, e.g., Übler et al. 2014). The stellar feedback effect in our simulations allows the formation of realistic disks. The M_s -to- M_{vir} ratios of the simulated galaxies are reasonable at all redshifts and the $z \sim 0$ properties of these galaxies are in good agreement with observations (see Colín et al. 2016).

The MW-sized galaxies are special because they are in the peak of the stellar mass growth efficiency within CDM halos, measured through the M_s -to- M_{vir} ratio (see for recent determinations e.g., Rodríguez-Puebla et al. 2017, and more references therein). For less massive galaxies, this efficiency decreases likely because of the global effects of SN-driven outflows, and for more massive ones, likely because of the long cooling times of the shock heated gas during the virialization of massive halos and the feedback from luminous AGNs (for a recent review on all of these processes, see Somerville & Davé 2015). Therefore, being MW-sized galaxies less susceptible to the effects of the not-well constrained stellar and AGN feedback processes, they are more suitable for exploring the predictions of Λ CDM-based simulations/models and for comparing them with observations.

1.2. Observational inferences

The observational study of the radial mass growth of *individual* galaxies is based mainly on fossil signals as the color, metallicity, and age gradients obtained from photometric, spectral energy distribution, and/or line-strength indices observations of local galaxies (for recent works, see e.g., Wang et al. 2011; Pan et al. 2015; Li et al. 2015; Dale et al. 2016; Kennedy et al. 2016; Lian et al. 2017). A more complete inference is provided by the fossil record method using Integral Field Spectroscopy (IFS) observations across the galaxies (Lin et al. 2013; Pérez et al. 2013; Ibarra-Medel et al. 2016; González Delgado et al. 2016; Goddard et al. 2017; García-Benito et al. 2017). There are also detailed stellar population studies based on color-magnitude diagrams obtained for the MW and nearby galaxies (e.g., Williams et al. 2009; Cheng et al. 2012; Boeche et al. 2014; Hayden et al. 2014; Mikolaitis et al. 2014). An alternative approach is to determine the instantaneous signal of the growth process, for example, by using the observational determination of the stellar and SFR density profiles (Muñoz-Mateos et al. 2007; Pezzulli et al. 2015). The radial growth modes inferred with this approach strictly refer only to the current time but under some assumptions can be extrapolated to some fraction of the past history of galaxies.

By using these different methods most of the authors have concluded that a significant fraction of the local galaxies formed (or are currently forming) their inner stellar masses earlier than their outskirts, that is, their stellar masses grow inside out. In more detail, several of these studies show that the mode and rate of radial mass growth may change with galaxy type, mass, environment, etc. For example, Ibarra-Medel et al. (2016) have found for a large sample of galaxies from the 'Mapping Nearby Galaxies at the Apache Point Observatory' (MaNGA) survey (Bundy et al. 2015), that blue/late-type galaxies follow, on average, a significantly more pronounced inside-out formation mode than red/early-type galaxies, with some evidence that the outer regions of the latter assembled more irregularly, likely due to minor mergers.

Under the assumption that stars form and remain in roughly the same position, the SF and mass growth histories inferred with the fossil record methods are expected to trace the radial stellar mass assembly of galaxies. However, this assumption should be taken with caution; a fraction of the stars could have been formed in other (secondary) galaxy(ies) that afterward merged with the primary one or the stellar mass could suffer radial net transport within the same primary galaxy by dynamical processes, in such a way that the inferred radial MGHs could trace with some bias the real (dynamical)

radial mass assembly of galaxies. It is currently a matter of debate how significant are these processes in galaxies, in particular, whether they produce a dramatic radial mass redistribution or just mix at small scales the stellar populations increasing the width of the metallicity distribution with age (e.g., Sellwood & Binney 2002; Debattista et al. 2006; Roškar et al. 2008; Schönrich & Binney 2009; Roškar et al. 2012; Berrier & Sellwood 2016). Here, using our simulations, we will explore how different can be the radial archaeological MGHs from the real (current) ones to evaluate the possible effects of radial mass redistribution by internal dynamical processes.

The radial mass assembly of galaxies has been also estimated from look-back time observations of a given galaxy population (for example, massive or MW-like galaxies) and by using the stacking technique for the selected galaxy population at each redshift bin in order to get the average evolution (van Dokkum et al. 2010, 2013). For the progenitors of MW-sized galaxies, van Dokkum et al. (2013) have found that the mass contained inside 2 kpc grows on average slower than the mass outside this radius since $z \sim 2$; even more, since $z \lesssim 0.6$, the inner mass growth stops at all, while the outer mass continues growing. By means of this kind of direct look-back time studies, as well as semi-empirical approaches, it was also confirmed that the effective radius of the MW-sized progenitors increase with time but slowly, which implies a mild inside-out growth (e.g., van Dokkum et al. 2013; Patel et al. 2013; Papovich et al. 2015; Rodriguez-Puebla et al. 2017).

The content of this paper is as follows. Section 2 briefly describes the simulations and the main properties of the simulated galaxies. Section 3 presents the half-mass radius and global/radial stellar mass growth of the galaxies, using different ways to account for the accumulation or loss of stellar mass in the radial bins. In Section 4, we present a study of the SF regime in the innermost galaxy regions compared to the whole galaxy in order to inquire about an inside-out quenching process that adds to the structural inside-out mass growth. In Section 5, we compare our results with inferences from recent observations, both based on the fossil record method applied to local galaxies and on look-back time observations of MW-size selected galaxy populations. Section 6 is devoted to discuss our results and their comparisons with observations. We summarize and present our conclusions in Section 7. In Table 1 the acronyms and definitions used in this paper are defined.

2. THE SIMULATIONS

The suite of eight MW-sized simulations to be studied here were presented and discussed in Colín et al. (2016,

Table 1. A list of acronyms and definitions used in this paper

AGN	Active Galactic Nucleus
CANDELS	Cosmic Assembly Near-IR Deep Extragalactic Legacy Survey
IFS	Integral Field Spectroscopy
IMF	Initial Mass Function
Λ CDM	Lambda Cold Dark Matter
MaNGA	Mapping Nearby Galaxies at the APO
MGH	(Stellar) Mass Growth History, $M_s(< t)$
-- current	Total stellar mass accumulated with time in a given region (Eq. 1)
-- in-situ	Stellar mass accumulated w/time only from particles formed in the given region (Eq. 1 w/o $M_{*,in}$, $M_{*,out}$)
-- archaeo-logical	Cumulative stellar mass distribution as a function of age from particles at $z \sim 0$ in a given region
MW	Milky Way
SDSS	Sloan Digital Sky Survey
SFR	Star Formation Rate
sSFR	Specific Star Formation Rate
SN	Supernova
Sp#D	Name of the runs, D stands for disk-dominated
Sp#L	Name of the runs, L stands for lenticular-like
Sp#S	Name of the runs, S stands for spheroid-dominated
D/T	Disk-to-total stellar mass ratio (dyn. determined)
M_s	Total galaxy stellar mass (within $0.1R_{vir}$)
M_{vir} , R_{vir}	Virial mass and radius
$R_{0.5}$	Stellar half-mass radius
t_{depl}	Depletion time (timescale at which the cold gas is consumed given the current SFR)
t_{lb}	Look-back time
$\langle t_{lb} \rangle_{mw}$	Mass-weighted average look-back time from a given MGH
Δt_{i-o}	Difference in $\langle t_{lb} \rangle_{mw}$ at $0-0.5R_{0.5}$ and $1-1.5R_{0.5}$
t_{sf}	Timescale at which the stellar mass is duplicated keeping constant the current SFR (inverse of sSFR)
V_{max}	Maximum circular velocity

see for details therein). The simulations were run using the N-body + Hydrodynamic Adaptive Refinement Tree (ART) code (Kravtsov, Klypin & Khokhlov 1997; Kravtsov 2003; Kravtsov, Nagai & Vikhlinin 2005), which incorporates a variety of physical processes such as gas cooling, SF, stellar feedback, advection of metals, and a UV heating background source. The Compton heating/cooling, atomic and molecular cooling, and UV heating from a cosmological background radiation (Haardt & Madau 1996), are all included in the computation of the cooling/heating rates. These are tabulated for a temperature range of $10^2 < T < 10^9$ K and a grid of densities, metallicities, and redshifts using the

CLOUDY code (Ferland et al. 1998, version 96b4). Stellar particles are formed in the gas cells with $T < 9000$ K and $n_g > 1\text{cm}^{-3}$, where T and n_g are the temperature and number density of the gas, respectively. A stellar particle of mass $m_* = \epsilon_{\text{SF}} \times m_g$ is placed in a grid cell every time the above conditions are simultaneously satisfied, where m_g is the gas mass in the cell and ϵ_{SF} is a parameter. We have set $\epsilon_{\text{SF}} = 0.65$. This and the other subgrid parameters were found in Roca-Fàbrega et al. (2016, see also Avila-Reese et al. 2011) to be optimal within the context of our subgrid recipes for the given minimal spatial resolution attained in our simulations ($109 h^{-1}\text{pc}$) and the integration time steps.

An “explosive” stellar thermal feedback recipe was used. Each stellar particle deposits into its parent cell $E_{\text{SN}+\text{Wind}} = 2 \times 10^{51}$ erg of thermal energy for each star more massive than $M_* = 8 M_\odot$ (half of this energy is assumed to come from the type-II SNe and half from the shocked stellar winds) and a fraction $f_Z = \min(0.2, 0.01M_* - 0.06)$ of their mass as metals. The code also accounts for the SN Ia feedback assuming a rate that slowly increases with time and broadly peaks at the population age of 1 Gyr. A fraction of 1.5×10^{-2} of mass in stars between 3 and $8 M_\odot$ explodes as SNe Ia over the entire population history and each SN Ia ejects $1.3 M_\odot$ of metals into the parent cell. For the assumed Miller & Scalo (1979) IMF (M_* in the range 0.1–100 M_\odot), a stellar particle of $10^5 M_\odot$ produces 749 SNe II (instantly) and 110 SNe Ia (over several billion years). On the other hand, stellar particles return a fraction of their mass and metals to the surrounding (stellar mass loss).

The thermal energy, suddenly dumped into the cell, raises the temperature of the gas cell to values $\gtrsim 10^7$ K. Although, as a receipt to avoid overcooling (see e.g., Stinson et al. 2006), we have disabled the radiative cooling for some time (40 Myr) in those cells where young stellar particles are located, this is almost not necessary in our simulations because for the typical densities and temperatures found in the SF cells, immediately after the formation of a stellar particle ($\gtrsim 1\text{cm}^{-3}$ and $T \gtrsim 10^7$ K), the cooling time is actually longer than the crossing time (Dalla Vecchia & Schaye 2012). Therefore, in most of the cases the gas in the cell, where the newborn stellar particle is located, expands to the neighbor cells before radiating away its heat.

The simulations were performed for the Λ CDM cosmology, with $\Omega_m = 0.3$, $\Omega_\Lambda = 0.7$, and $\Omega_b = 0.045$. The CDM power spectrum was taken from Klypin & Holtzman (1997) and it was normalized to $\sigma_8 = 0.8$, where σ_8 is the rms amplitude of mass fluctuations in $8 h^{-1}\text{Mpc}$ spheres. First, eight halos of present-day masses around

$10^{12} M_\odot$ were chosen from a low-resolution N-body dark matter-only ART simulation, run in a box of $50\text{Mpc}/h$ on a side. Except for one halo, which has a companion of comparable mass at a distance of $0.26 h^{-1}\text{Mpc}$, all the others are relatively isolated at $z \sim 0$. Thus, the environment of the simulated galaxies should not be associated to one of groups/clusters and can be related to what observers call the field. The eight selected regions were resimulated with much higher resolution and including baryons with the N-body + Hydrodynamics ART code. The maximum level of refinement was set to 12 so that the high density regions are mostly filled, at $z = 0$, with cells of $109 h^{-1}\text{pc}$ per side; this is the nominal spatial resolution of our simulations. The number of dark matter particles in the high-resolution zone, where galaxies are located, ranges from about 1.5 to 2 million and the particle mass is $1.02 \times 10^6 h^{-1}M_\odot$. On the other hand, the number of stellar particles in the galaxies at $z = 0$ ranges from 1.2 to 5.1×10^5 .

Colín et al. (2016) have determined the kinematic spheroid-to-disk mass ratio at $z = 0$ by means of two methods. The results were close in both cases. From these results, we may classify the simulated galaxies as: disk dominated, highlighted with the final letter D (runs Sp3D, Sp1D, Sp7D, and Sp8D), lenticulars like (with spheroid-to-disk ratios not too different, highlighted with the final letter L; Sp2L and Sp6L), and spheroid dominated (highlighted with the final letter S; Sp4S and Sp5S). The two latter runs are spheroid dominated because they have undergone late major mergers; during these late mergers the galaxies had bursts of SF and at $z = 0$ they are yet forming stars (5.6 and $1.4 M_\odot/\text{yr}$, respectively); they would correspond to the rare cases of blue, star-forming early-type local galaxies. Aside from these two runs, the general evolutionary picture for the other runs is that at high redshifts ($z > 1-2$) the disks were turbulent, with high vertical gas velocity dispersions and intense bursts of SF, but since $z \sim 1$, the galaxies evolve quiescently, with relatively low SFRs and growing stable gaseous disks (Colín et al. 2016).

In Colín et al. (2016) were presented the main properties of the eight simulated galaxies (see Table 1 therein). In our Table 2 we reproduce some of these properties. The runs are ordered from the largest to the lowest disk-to-total mass ratio D/T at $z = 0$ (column 5). The $z = 0$ stellar masses range from ≈ 2 to $8 \times 10^{10} M_\odot$, and their stellar half-mass radii, from 2.6 to 6.8 kpc. The galaxies are only slightly above the $V_{\text{max}} - M_s$ observed relation but mostly within the intrinsic scatter around this relation. Their radii and cold gas fractions are also in rough agreement with observations given their masses. The rotation curves of all the galaxies are nearly flat, with

Table 2. Some properties of simulated galaxies^a

(1)	(2)	(3)	(4)	(5)	(6)	(7)
Run	M_{vir}	M_s	$R_{0.5}$	D/T	“Morph”	Δt_{i-o}
	$10^{12} M_{\odot}$	$10^{10} M_{\odot}$	kpc			(Gyr)
Sp3D	0.99	5.3	6.4	0.81	disk-dom	3.29
Sp1D	0.84	1.8	6.0	0.75	disk-dom	2.06
Sp7D	1.09	5.4	5.2	0.69	disk-dom	2.04
Sp8D	1.20	6.3	5.9	0.64	disk-dom	3.37
Sp2L	0.83	3.3	4.9	0.43	lentic.	1.18
Sp6L	0.97	2.3	2.6	0.30	lentic.	2.53
Sp4S	1.56	8.4	6.8	0.25	sph-dom	0.80
Sp5S	1.05	4.1	3.3	0.09	sph-dom	0.02

^a See definitions in Table 1.

V_{max} values from 165 to 226 km/s. The stellar-to-halo mass ratios at $z \sim 0$ are in agreement (within the 1σ scatter) with direct and semi-empirical determinations.

3. THE STRUCTURAL ASSEMBLY AND STELLAR MASS GROWTH HISTORIES

3.1. Evolution of the stellar half-mass radius

Figure 1 presents the evolution of the stellar half-mass radius, $R_{0.5}$, for the eight MW-sized simulations: upper panel for the disk-dominated galaxies and lower for the spheroid-dominated ones. The radii were normalized to their $z = 0$ values. In all the cases $R_{0.5}$ grows rapidly with time. For example, for the disk-dominated galaxies, $R_{0.5}$ at $z = 1$ is $\approx 0.3 - 0.5 R_{0.5}$ at $z = 0$. As mentioned in the Introduction, the structural growth of disks formed from gas that initially follows the Λ CDM halo mass and angular momentum distributions, and that cools and settles down in centrifugal equilibrium conserving angular momentum, happens the inside out. The thick gray dashed line in figure 1 corresponds to such kind of predictions for a $\approx 10^{12} M_{\odot}$ present-day halo (Firmani & Avila-Reese 2009, see also e.g., Somerville 2009); in this model, the SF in the disk is triggered by the Toomre gas gravitational instability criterion and selfregulated by a balance between the energy input due to SNe and the turbulent energy dissipation in the ISM; the Kennicutt-Schmidt relation is naturally recovered by the model.

Our numerical results for the disk-dominated galaxies, show a faster $R_{0.5}$ evolution up to $z = 1 - 2$ than the predicted for the simple Λ CDM-based galaxy evolutionary models. While this could be by many reasons, a possibility is that in simulations, apart from the structural inside-out growth of stellar mass, an inside-out quench-

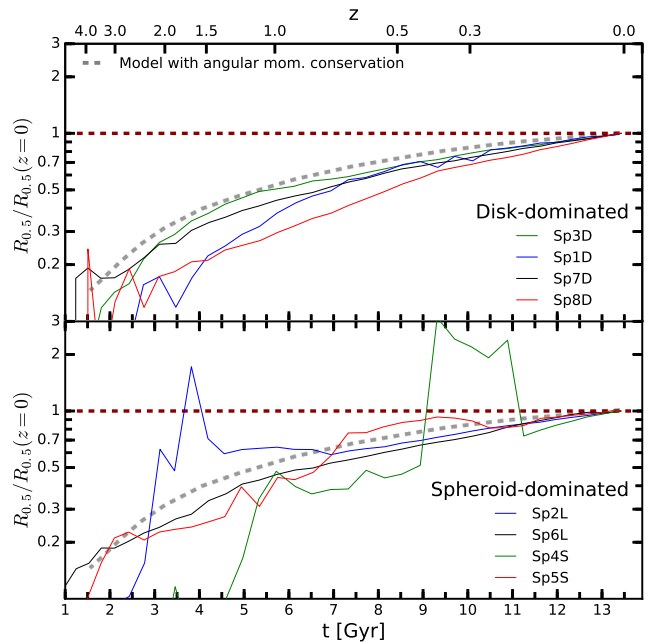


Figure 1. Normalized half-mass radius evolution of the disk-dominated (upper panel) and spheroid-dominated (lower panel) galaxies. The normalization is with respect to the $R_{0.5}$ values at $z = 0$. The gray line shows the $R_{0.5}$ evolution from a Λ CDM-based galaxy evolutionary model (detailed angular momentum conservation is assumed) corresponding to a present-day halo of $10^{12} M_{\odot}$ (Firmani & Avila-Reese 2009).

ing of SF happens. In this case, the inner regions slow down or totally quench the SF first, braking their stellar mass growth, while the outer regions keep forming stars, in such a way that their stellar masses grow now faster than in the inner regions; as the result, $R_{0.5}$ increases more rapid with time. We will see below that this indeed happens in most of the runs. For the lenticular-like and spheroid-dominated galaxies, $R_{0.5}$ has periods of increase and decrease related to the mergers, excepting run Sp6L that does not suffer mergers since early epochs.

3.2. Global and radial stellar mass growth histories

Our main goal is to study the global and radial stellar mass growth of the simulated MW-sized galaxies in the context of the Λ CDM cosmology. We dissect the galaxies at any time in cylindrical bins with radii $(0, 0.5)$, $(0.5, 1)$, $(1, 1.5)$, and $(1.5, 2) R_{0.5}(0)$ ¹ and height ± 2 kpc above the disk plane. Then, we measure within these

¹ $R_{0.5}(0)$ is the present-day stellar half-mass radius. We have chosen these radial bins in order to compare them with observational inferences (Section 5).

fixed bins the accumulation of stellar mass in three different ways:

(1) *Current (real) mass growth histories (MGHs)*, defined as the stellar mass accumulated at each snapshot (redshift) within the radial bins. These histories account for the amount of mass in stellar particles added or subtracted at each radial bin between two snapshots (epochs):

$$\Delta M_* = M_{*,\text{in-situ}} + M_{*,\text{in}} - M_{*,\text{out}} - M_{*,\text{ml}}, \quad (1)$$

where $M_{*,\text{in-situ}}$ is the mass in stellar particles formed in the bin (in situ), $M_{*,\text{in}}$ is the mass in stellar particles that came from other radial bins or from outside the galaxy (by mergers, for instance), $M_{*,\text{out}}$ is the stellar mass in particles that left the radial bin, and $M_{*,\text{ml}}$ is the mass loss by winds suffered by the stellar particles in the bin depending on their formation epochs and the current time.

(2) *In-situ stellar MGHs*, defined as the stellar mass accumulated by stellar particles formed only in situ at each radial bin, not taking into account gained or lost stellar particles from/to other regions (but taking into account the stellar mass loss of the in-situ formed stellar particles). This is equivalent to Eq. (1) without the terms $M_{*,\text{in}}$ and $M_{*,\text{out}}$. Note that the in-situ MGH is related to the *cumulative SF history* typically used in the literature.

(3) *Archaeological MGHs*, constructed from the information of the stellar particles in the last snapshot ($z = 0$), that is, in this case we do not use the historical information contained in previous snapshots. For each stellar particle at $z = 0$, we know its formation time (age), its initial mass, and the account of mass lost by winds as a function of time. Therefore, from the distribution of stellar mass fractions as a function of age (look-back time) in a given region of the $z = 0$ galaxy we can calculate the accumulated stellar mass at each look-back time in that region. This is conceptually similar to the observational determinations obtained by means of the fossil record method (see e.g., Pérez et al. 2013; Ibarra-Medel et al. 2016; Goddard et al. 2017); since in this case the information comes only from the observed stellar populations, it is not immediate to know whether stars were formed at the “observed” position or in other regions.

Following, we present the three types of MGHs described above for each one of our eight MW-sized galaxy simulations. The radial MGHs are *normalized* to their corresponding masses at $z = 0$ in such a way that the relative growth rates among different radial bins and different galaxies can be compared. In this sense, the figures show rather than the absolute mass contribution

of each radial bin, *the rate at which the mass grows in each bin*. The panels in the figures to be shown below are ordered from the most to the least disk-dominated galaxies at $z = 0$.

Current stellar MGHs: Figure 2 presents these MGHs for each one of the radial bins defined above (solid lines) as well as for the total galaxy (thick gray lines). In all the cases, the inner radial bins accumulate most of the time earlier their stellar masses than the outer bins, that is, the mass growth is the inside out. The most pronounced inside-out trends are for the disk-dominated galaxies, specially Sp7D and Sp8D, while the least pronounced trends are for the spheroid-dominated Sp4S and Sp5S galaxies, which suffered late major mergers. At some epochs, the mass fractions in a given radial bin can decrease. This is most evident in the Sp4S and Sp5S galaxies, at epochs before or during their major stellar mergers; strong radial mass redistribution processes take place during this phase and finally the mass increases at all radii significantly due to both the addition of stellar particles from the secondary galaxy and to enhanced in-situ star formation (see below).

The horizontal dotted lines in figure 2 indicate when each radial bin, or all the galaxy, has attained 50, 70, and 90 per cent of the respective $z = 0$ stellar mass. The assembly time differences between the innermost radial bin ($0-0.5R_{0.5}$) and the outer bin ($1-1.5R_{0.5}$) for the corresponding mass fractions of 70 per cent, $\Delta t_{\text{in-out}}(70\%)$, are 1.63, 4.40, 2.40, and 3.84 Gyr for the disk-dominated Sp3D, Sp1D, Sp7D, and Sp8D galaxies, respectively, showing a clear inside-out behavior. These assembly time differences are lower for the spheroid-dominated galaxies, excepting for Sp6L, which shows a pronounced inside-out mass assembly.

For all the simulated galaxies, but Sp4S and Sp5S, the innermost regions ($0 - 0.5R_{0.5}$) suddenly slow down or cease at all their stellar mass growth since early look-back times that range from ≈ 10 Gyr (Sp7D and Sp6L) to ≈ 6 Gyr (Sp2L, Sp3D). This change in the stellar mass growth velocity is also observed in the outer regions but it is typically more gentle and delayed to later epochs than in the innermost regions. This behavior could be due to preferential late stellar mass accretion (mergers) in the outer regions or to significant radial mass redistribution from inside out. However, as we will see below, the main reason is that galaxies, besides the structural inside-out growth, suffer an inside-out SF quenching.

In-situ stellar MGHs: Figure 3 is as figure 2 but for the in-situ MGHs or cumulative SF histories.

By comparing the in-situ and current radial normalized MGHs we find little differences, which shows that

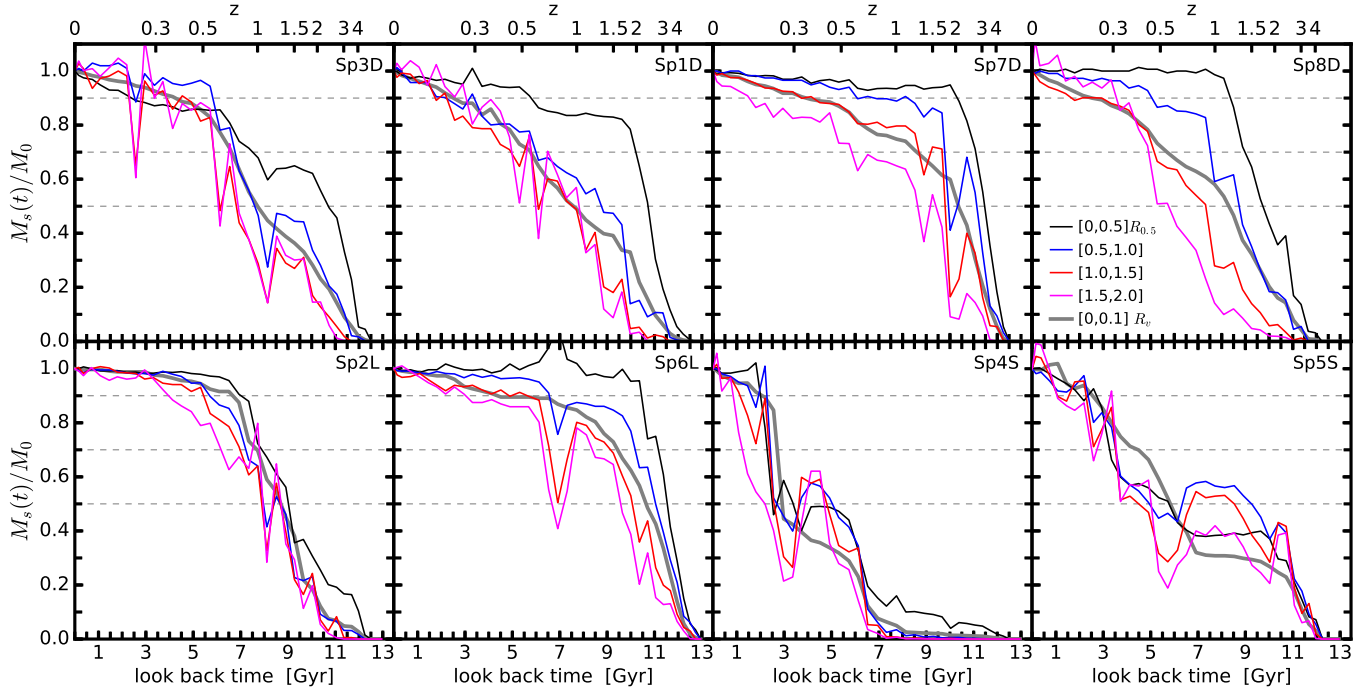


Figure 2. Global (gray line) and radial (colored lines) current MGHs for the eight simulated galaxies. The color code of each radial bin is plotted in the inset of the upper right panel. Each MGH is normalized to the present-day stellar mass contained in the respective radial bin or in the whole galaxy. The radial bins are defined in terms of $R_{0.5}$ as measured at $z = 0$ and they remain the same in physical unities at all redshifts. The current MGHs account for the stellar mass directly measured at each epoch. From left to right and from top down the kinematical disk-to-total mass ratio of the galaxies decreases.

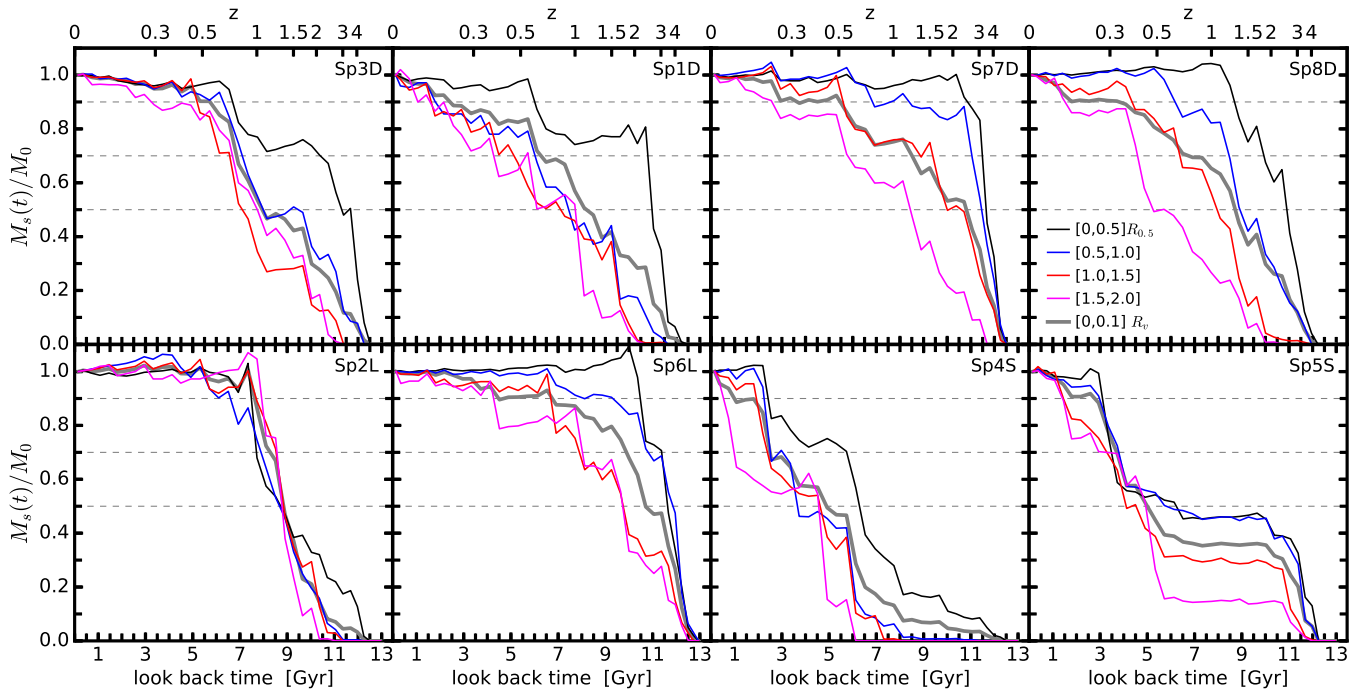


Figure 3. As in figure 2 but for the in-situ MGHs. The in-situ MGHs account only for the mass accumulated in stellar particles formed in the galaxy or in the given radial bin, taking into account the stellar mass loss by winds but not the loss or gain of ex-situ stellar particles.

the radial stellar mass growth of the simulated galaxies is mainly driven by in-situ SF, without significant contri-

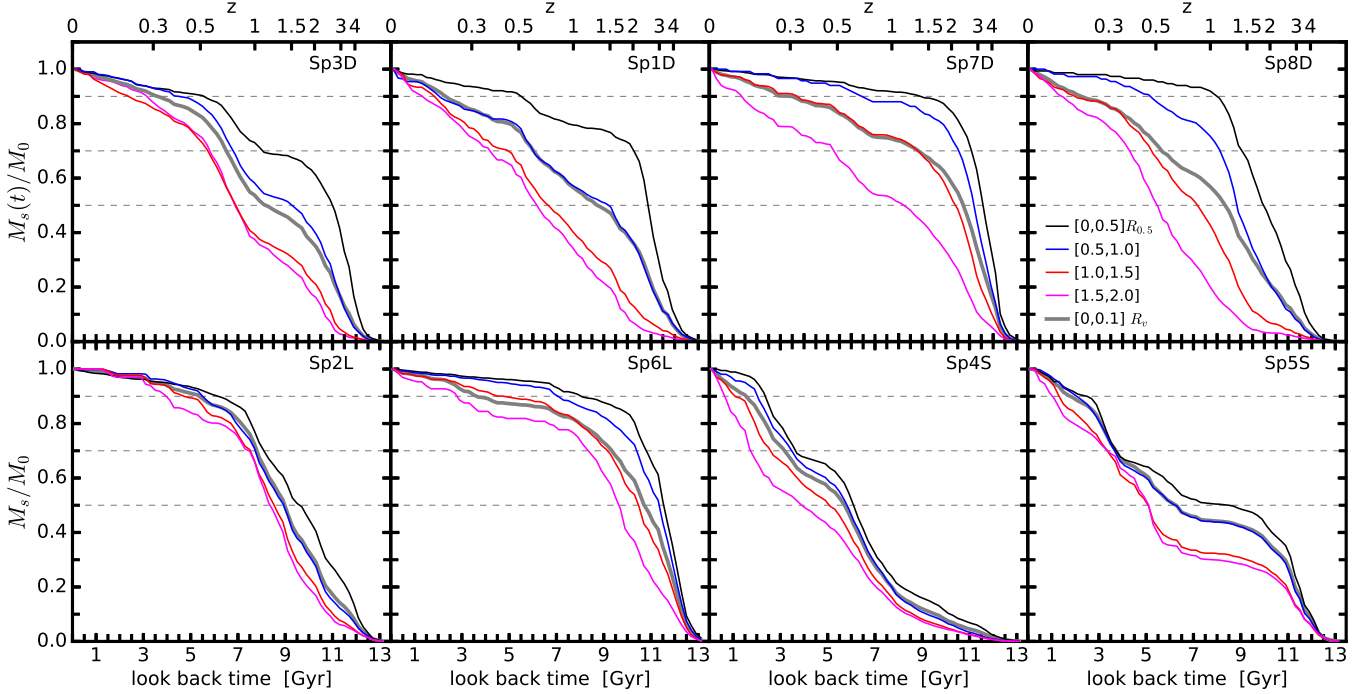


Figure 4. As in figure 2 but for the archaeological MGs. The archaeological MGs are constructed from the age distributions of the stellar particles measured at $z = 0$. These MGs can be compared to the fossil record inferences from IFS observations.

bution of mergers and/or large-scale radial mass flows. In more detail, the current inner normalized MGs in most of the cases are slightly shifted to lower fractions at a given time than the corresponding in-situ MGs. This is mainly because, apart from the growth by in-situ SF, the (inner) stellar mass assembles by some accretion events (minor mergers, which in spiraling motion tend to fall to the galaxy center). The normalized current MGH shifts to a lower mass fraction with respect to the normalized in-situ MGH each time a merger happens. Some (little) large-scale radial mass flows are also possible, contributing this to make slightly different the current and in-situ MGs.

The in-situ normalized MGs show that SF and its quenching in the simulated galaxies proceeds inside out, even in the Sp4S and Sp5S runs (where late major mergers happened): the in-situ cumulative SF at early epochs grows faster in the inner regions than in the outer ones, but then, the in-situ SF suddenly slows down or even quenches completely in the innermost ($0-0.5 R_{0.5}$) regions while the outer ones keep yet increasing their masses due to in-situ SF. The only exception is run Sp2L, which shows a nearly radially homogeneous mass growth by in-situ SF, with periods of even outside-in SF. As it will be seen in Section 4, the SF in this galaxy becomes very inefficient in its outer regions.

In Appendix A, we present complementary evidence of the strong inside-out growth of the simulated galaxies:

we show the evolution of the radial cumulative mass distribution of in-situ formed stars, and the comparison of the measured total radial stellar mass distributions with the ones of the in-situ formed stars. Further, in Appendix B we explore the net radial transport of stellar particles (only for the Sp8D and Sp6L runs) and find that they may displace on average up to 1-2 kiloparsecs away (1σ) from their birth place but roughly in both radial directions, not causing such a significant global mass redistribution.

Archaeological stellar MGs: Figure 4 is as figures 2 and 3 but for the archaeological stellar MGs constructed from the age distributions of the stellar particles measured at $z = 0$. In general, these radial MGs are very similar to the current ones, which shows that neither mergers nor global radial stellar transport affect too much the radial structural evolution of our Λ CDM simulated MW-sized galaxies. Only during the major mergers in the Sp4S and Sp5S runs the normalized archaeological radial MGs differ significantly from the current ones. The archaeological MGs always increase while the current MGs may decrease and then suddenly increase due to radial mass redistribution and mass accretion during galaxy interactions and mergers. The archaeological radial MGs can be compared to the fossil record inferences from IFS observations (see Section 5).

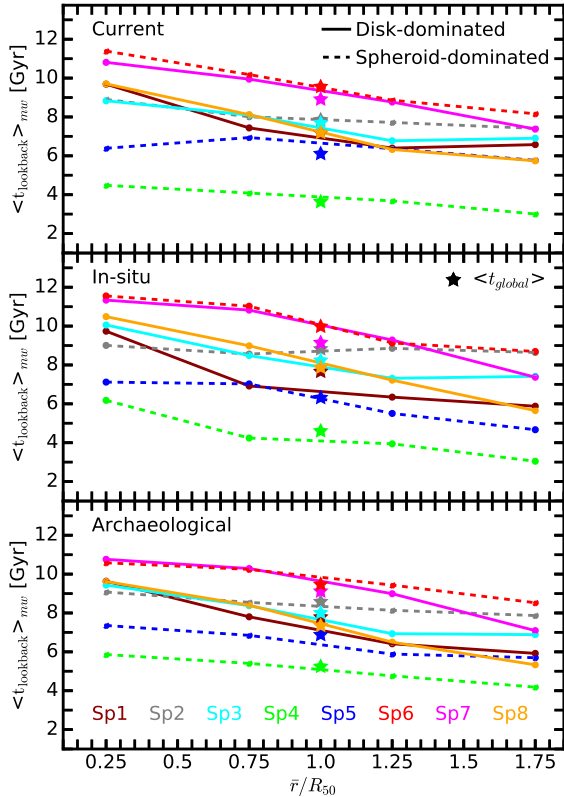


Figure 5. Average mass-weighted look-back times of each one of the radial bins used in figures 2–4 (solid lines and dashed lines are for the disk- and spheroid-dominated galaxies, respectively). From top to bottom, the “age” profiles correspond to the current, in-situ, and archaeological MGHs, respectively. The stars indicate the corresponding global average mass-weighted look-back times.

3.3. Quantifying the radial stellar mass assembly

The different radial MGHs plotted in figures 2–4 show that the simulated MW-sized galaxies assemble (driven mostly by in-situ SF) and slow down/quench their SF the inside out. To quantify and compare the radial differences in the normalized stellar MGHs of galaxies, we calculate the average look-back time of each one of the radial MGHs, $\langle t_{\text{lb}} \rangle_{\text{mw}}$, that is, we collapse the given cumulative mass track into an unique quantity. This is calculated as the sum of each snapshot look-back time weighted by the fraction of the stellar mass increased/decreased since the previous snapshot. In figure 5, for each simulated galaxy, we plot $\langle t_{\text{lb}} \rangle_{\text{mw}}$ for the four radial bins used in previous subsections. From top down, the panels are for the current, in-situ, and archaeological MGHs. Note that in the last case, $\langle t_{\text{lb}} \rangle_{\text{mw}}$ is related to the mean mass-weighted age of the stars in the given radial bin. Solid (dashed) lines are for the disk- (spheroid-)dominated galaxies. The

current, in-situ, and archaeological mass-weighted ages of the whole galaxy are shown for each run with a star in the corresponding panels of figure 5.

The average mass-weighted look-back times decrease in general with radius: the stellar mass assembly and its braking happened earlier in the inner regions than in the outer ones. Such inside-out trends are similar for the current, in-situ, and archaeological MGHs. In general, the average times are slightly higher (older ages) for the in-situ MGHs than for the current MGHs. As discussed above, this is mainly because the current MGHs, besides the stellar particles formed in situ, take into account the accretion of ex-situ particles (some of them coming from relatively late mergers); that is, the current MGHs refer both to the intrinsic SF and the (dynamical) stellar mass assembly in the given region. The main differences between the in-situ and current average times are namely for runs Sp4S and Sp5S, which suffer late major mergers.

The disk-dominated galaxies have the steepest $\langle t_{\text{lb}} \rangle_{\text{mw}}$ profiles. For the current MGHs, the average mean look-back times of the $0 - 0.5R_{0.5}$ radial bin range from ≈ 8.8 to 10.8 Gyr, while these times for the $1 - 1.5R_{0.5}$ radial bin range from ≈ 6.4 to 8.8 Gyr. The time differences for each galaxy, Δt_{i-o} , range from ≈ 2 to 3.4 Gyr (see column 7 of Table 2); these time differences in the case of the in-situ and archaeological MGHs are very similar.

Interesting enough, the run Sp6L, while spheroid-dominated, also shows a pronounced inside-out formation ($\Delta t_{i-o} = 2.5$ Gyr); this is actually the earliest formed galaxy among all the runs and its large spheroid is probably the result of long disk secular evolution since this galaxy did not suffer significant mergers across its evolution. On the other hand, the runs Sp4S and Sp5S, which are spheroid-dominated and suffered recent major mergers, show small time differences among the different radial bins; these galaxies are the latest assembled in our suite of simulations. The run Sp2L is the one with the flattest $\langle t_{\text{lb}} \rangle_{\text{mw}}$ profiles; for the in-situ profile, the outer regions are even slightly older than the inner ones.

The mean look-back times of the radial archaeological MGHs are in most of the cases slightly older (typically by < 0.5 Gyr) than those of the current MGHs. The largest differences are for the run Sp4S, up to 1.5 Gyr at all radii. Since this galaxy has suffered a recent major merger, its stellar mass assembly (with contribution of accreted ex-situ stars) is younger on average than the ages of the stars that compose this galaxy at $z = 0$. So, in the cases where galaxies suffered late major mergers, the archaeologically inferred MGHs and average mass-weighted ages constrain their stellar mass assembly his-

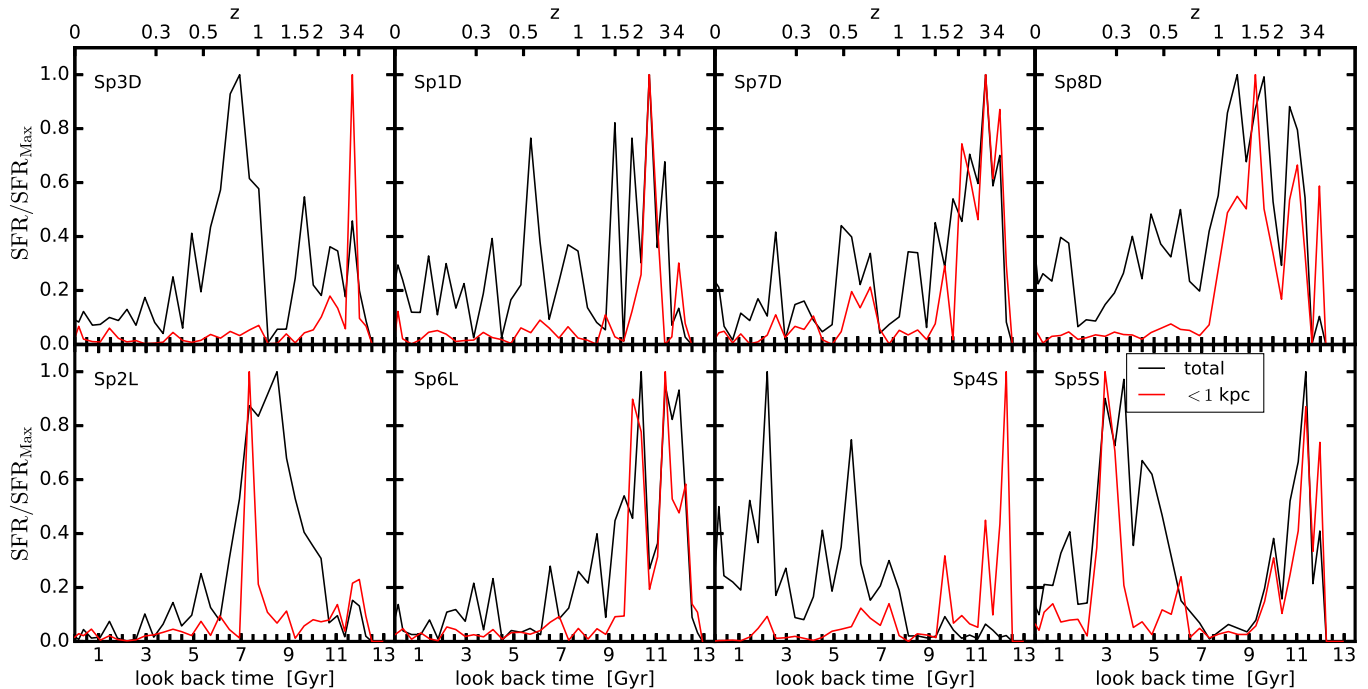


Figure 6. Evolution of the global SFR (black lines) and the SFR inside 1 kpc (red lines) of the simulated galaxies. The SFR’s are normalized to their corresponding maximum values. The SFR histories of the central regions tend to be qualitatively different to those of the whole galaxy.

tories with some shift to earlier epochs with respect to the real ones.

4. CENTRAL/GLOBAL STAR FORMATION AND GAS FRACTION HISTORIES

The radial stellar mass growth of our simulated galaxies is driven by in-situ SF. According to the radial in-situ MGHs presented in the previous Section, the inner regions tend to halt their mass growth at high redshifts. Following, we explore in more detail the SFR² history of the central 1 kpc region compared to the corresponding SFR history of the whole galaxy. Figure 6 displays these histories for the eight runs; black and red lines are for the central 1 kpc and the whole galaxy histories, respectively. To compare the shapes of both SFR histories, we have normalized them to their corresponding maximum values (the absolute SFR values within the small 1 kpc region are much lower than those of the whole galaxy). For most of the runs, the central 1 kpc region forms stars actively at early epochs (with fluctuations), and then the SFR strongly and abruptly decreases (quenches). Instead, the SFR histories of the whole galaxies present a less abrupt phase of final de-

creasing and show even some significant SF ‘bursts’ at later epochs (see for example, runs Sp3D, Sp1D and Sp8D). So, the SFR histories of the innermost regions are qualitatively different to those of the whole galaxy, in particular due to the early quenching of SF in the innermost regions. For runs Sp4S and Sp5S, the situation is slightly different since these galaxies suffered major mergers after $z \sim 1$.

We have measured also how the cold ($T \leq 1.5 \times 10^4$ K) gas-to-stellar mass ratio, $M_{g,cold}/M_s$, changes with time both for the whole galaxy and within the central 1 kpc. This ratio is related to the current gas reservoir and SF efficiency with respect to the past SF. By dividing both the numerator and denominator by the SFR, we have that $M_{g,cold}/M_s = t_{depl}/t_{sf}$, where $t_{depl} \equiv M_{g,cold}/\text{SFR}$ is the depletion or gas consumption time, and $t_{sf} \equiv M_s/\text{SFR}$ is the SF timescale at which the stellar mass duplicates if keeping constant the current SFR (t_{sf} is the inverse of the specific SFR, sSFR). When $t_{depl}/t_{sf} \sim 1$ or higher, there is a large gas reservoir and/or the SF process is very efficient. When $t_{depl}/t_{sf} \ll 1$, the gas reservoir is poor and/or the SF process becomes very inefficient as compared to the average past one. For example, for their high-redshift simulations of massive galaxies, Tacchella et al. (2016a) find that when the gas replenishment time becomes larger than $10 \times t_{depl}$, which roughly corresponds

² The SFR is measured as the mass sum of all the stars younger than 100 Myr at a given epoch divided by this time. We have experimented with other times (from 40 to 200 Myr) and the results are very similar in all the cases.

to $t_{\text{sf}} \gtrsim 11 \times t_{\text{depl}}$, then the SF process enters in a long-term quenching phase.

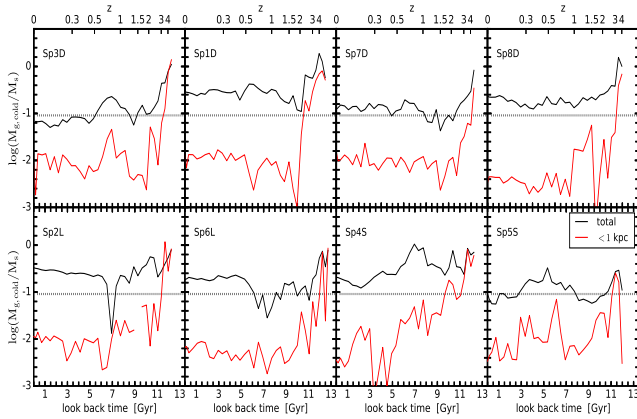


Figure 7. Evolution of the cold gas-to-stellar mass ratio ($M_{g,\text{cold}}/M_s = t_{\text{depl}}/t_{\text{sf}}$) inside 1 kpc (red lines) and for the whole galaxy (black lines). The horizontal dotted line indicate a value of $t_{\text{depl}}/t_{\text{sf}} = 1/11$. Below this value, the SF is expected to enter in a long-term quenching phase, see text.

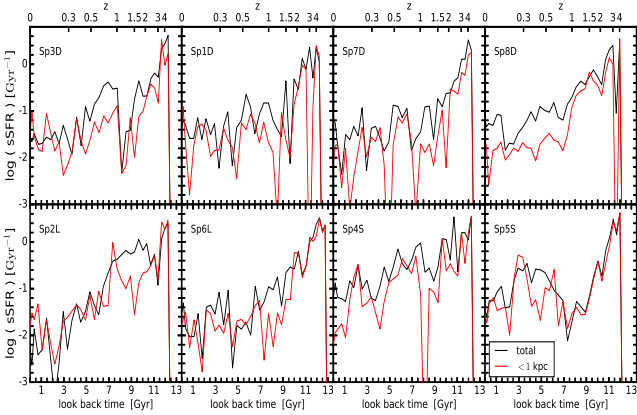


Figure 8. Evolution of the global sSFR (black lines) and the sSFR inside 1 kpc (red lines).

Figure 7 shows the evolution of $M_{g,\text{cold}}/M_s$ ($= t_{\text{depl}}/t_{\text{sf}}$) within the central 1 kpc (red line) and for all the galaxy (black line), for our 8 simulated MW-sized galaxies. At early times ($z \sim 4$), $M_{g,\text{cold}}/M_s \sim 1$ for both the inner 1 kpc and the whole galaxy. Galaxies are gaseous and in an active period of SF at these early times. However, in a relatively short time, $M_{g,\text{cold}}/M_s$ strongly decreases in the inner 1 kpc region, excepting in runs Sp4S and Sp5S, which suffer late major mergers. The horizontal dotted line in the panels indicates the value $M_{g,\text{cold}}/M_s = 1/11$. In the central 1 kpc regions, $M_{g,\text{cold}}/M_s$ falls below this value at redshifts from ~ 4 to ~ 2 , evidencing that the inner regions start to quench early. At late epochs, $z \lesssim 0.5$, the values of $M_{g,\text{cold}}/M_s$

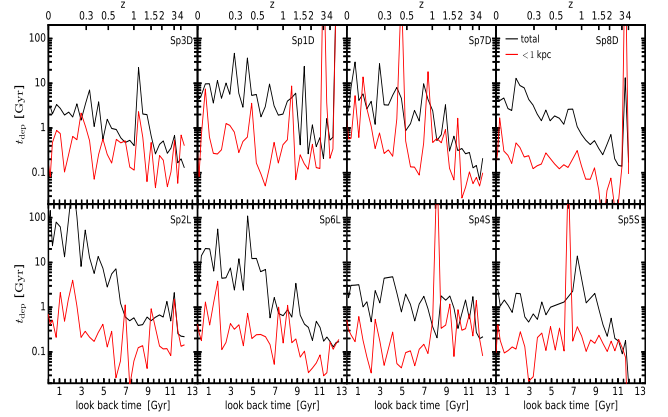


Figure 9. Evolution of the global depletion time (black lines) and the depletion time inside 1 kpc (red lines).

are ~ 0.01 or less; the innermost regions of the simulated galaxies entered into a long-term quenching phase. In contrast, the global $M_{g,\text{cold}}/M_s$ ratios show a slow decreasing with time and do not attain values below ~ 0.1 at $z \sim 0$, which suggests that the simulated galaxies are yet star-forming.

In Figure 8, the sSFR histories of the central 1 kpc (red line) and the whole galaxy (black line) are plotted. Both the inner (< 1 kpc) and global sSFR of the simulated galaxies are high at high redshifts: around 1 Gyr^{-1} or larger at $z > 3$, that is, both the global and inner stellar masses roughly duplicate by SF in $\lesssim 1$ Gyr. At lower redshifts, the sSFR strongly decreases. For the disk-dominated galaxies, the global sSFR decreases by roughly a factor of ten down to $z \sim 1$ and then continues decreasing but at a slower pace. At $z \sim 0$ these galaxies remain roughly as star forming, with values of sSFR around $2 - 5 \times 10^{-2} \text{ Gyr}^{-1}$. The sSFR values inside 1 kpc are lower than the global ones almost at all epochs. The largest difference is for Sp8D: the inner sSFR falls strongly since $z \sim 1$ and at $z < 0.5$ its value is on average $\lesssim 10^{-2} \text{ Gyr}^{-1}$ ($M_{g,\text{cold}}/M_s \lesssim 5 \times 10^{-3}$) while the global sSFR is on average three times larger. The Sp8D galaxy presents the most prominent inside-out mass assembly trend among all the simulated galaxies (see figures 2–4). Now we see that this is partially because the inner regions quench while the outer ones continue forming stars and growing in stellar mass. This implies that besides the structural inside-out mass growth, in our simulations there is an inside-out SF quenching process, which for Sp8D is very efficient. For the spheroid-dominated galaxies, the inner and total sSFR are close at all redshifts.

In Figure 9, the depletion time histories of the central 1 kpc (red line) and the whole galaxy (black line) are plotted. Both the inner and global galaxy depletion

times increase towards the present (excepting for Sp5S), showing that the simulated galaxies were more efficient in transforming gas into stars in the past. In all the cases, t_{depl} in the inner 1 kpc is shorter than for the overall galaxy, that is, the inner galaxy regions are more efficient in consuming gas into stars than the average of the whole galaxy. These differences tend to increase at lower redshifts. For the disk-dominated galaxies, at $z \sim 0.3 - 0$ the differences range from ≈ 0.4 to 1 dex. The inner depletion times of these galaxies are mostly shorter than 1 Gyr, though in some short periods they may jump to higher values. With these short depletion times, if there is no gas replenishment, then the central galaxy regions quench relatively fast. In some cases and at high redshifts, the depletion time inside 1 kpc can be lower than 100 Myr, approaching to the typical timescales of the processes governing the evolution of the interstellar gas. Numerical simulations of gaseous galactic disks show that star-forming molecular clouds may form on timescales shorter than a few 10^7 yr (Dobbs, Pringle & Burkert 2012; Dobbs, Pringle & Duarte-Cabral 2015). Therefore, in the central 1kpc region of our galaxies and at high redshifts, the SF can be as efficient as within the environment of molecular clouds. For the spheroid-dominated galaxies, the differences in t_{depl} between the inner regions and the overall galaxy are larger than for the disk-dominated galaxies, specially for lenticular-like galaxies Sp2L and Sp6L.

The Sp2L galaxy shows a behavior different to the rest of the runs. The whole galaxy becomes very inefficient in consuming gas into stars (the global t_{depl} increases with cosmic time up to ≈ 100 Gyr at $z \sim 0$) in spite that the gas is available; this galaxy ends with the highest gas-to-stellar mass ratio among all the simulations, $M_{g,\text{cold}}/M_s=0.35$. However, in its inner regions t_{depl} remains with values around 1-2 Gyr since $z = 0.5$, showing that the outer regions are those that become with time very inefficient in transforming gas into stars; this “outside-in” behavior in the gas transformation efficiency into stars compensates the structural inside-out growth, and as the result, the radial stellar mass growth of this galaxy, especially the in-situ one, is nearly homogeneous and even with periods of outside-in assembly trends (see figures 3, 14, and 5).

5. COMPARISON WITH OBSERVATIONAL INFERENCE

Our simulations of “field” MW-sized galaxies formed inside growing Λ CDM halos make concrete predictions about how the stellar mass is radially assembled across cosmic time. The half-mass radius grows fast with time and the radial stellar mass assembly is inside-out and

driven mainly by in-situ SF/quenching. From the empirical point of view, there have been several attempts to infer how is the radius and radial stellar mass growth of galaxies, specially the MW-sized ones (see Introduction). Following we present some of these inferences and attempt to compare with our theoretical results. We calculate the average of the global and radial MGHs for two types of MW-sized galaxies in our simulations: spirals (Sp1D, Sp3D, Sp7D, and Sp8D) + lenticulars (Sp2L and Sp6L), and highly spheroid dominated (Sp4S and Sp5S). The latter are spheroid dominated due to late major mergers, which produced also late bursts of SF (see figure 6). Therefore, these galaxies can be associated to observed blue, star-forming early-type galaxies, which are rare in the local universe and are located in isolated environments (see Lacerna et al. 2016, and more references therein).

5.1. Fossil record inferences

Ibarra-Medel et al. (2016) have presented the normalized radial MGHs of the first release of MaNGA galaxies (SDSS Collaboration et al. 2016) using the fossil record method implemented in the specialized pipeline analysis software called Pipe3D (Sánchez et al. 2016a,b). Here we present the average normalized MGHs as in Ibarra-Medel et al. (2016)³ in the same stellar mass range of our simulations, $2 - 8 \times 10^{10} M_{\odot}$,⁴ and for two groups: spiral + lenticular galaxies (morphological type $T \geq 0$) to be compared with the average of runs Sp1D, Sp3D, Sp7D, Sp8D, Sp2L, and Sp6L, and blue, star-forming early-type ($T < 0$) galaxies, to be compared with the average of runs Sp4S and Sp5S (see above). The morphological classification of MaNGA galaxies has been performed by eye with some complementary criteria (see Ibarra-Medel et al. 2016), and the criteria of blue and star-forming galaxies are based on the color and sSFR distributions of SDSS galaxies as a function of M_s (see Lacerna et al. 2014, 2016).

As explained in Ibarra-Medel et al. (2016), in order to calculate the average normalized MGHs, one needs to fix a given limit redshift, z_{lim} , at which the final respective stellar mass is defined for each galaxy. If z_{lim} is too low, then too few galaxies are left (the average red-

³ We use here a larger sample of MaNGA galaxies from the second data release (Abolfathi et al. 2017) and with the updated data reduction pipeline (Law et al. 2016), which improved the spectrophotometric calibration of galaxies.

⁴ The stellar masses in Pipe3D are calculated by assuming a Salpeter initial mass function. We shift these masses by -0.24 dex to correct to a Chabrier (Chabrier 2003) initial mass function, which is close to the the Miller & Scalo (1979) one used in our simulations.

shift of the MaNGA galaxies is around 0.035), and if z_{lim} is too high (in such a way that all the observed galaxies are included), then the late evolution (last ~ 2 Gyr for $z_{\text{lim}} = 0.15$) of most of observed galaxies is lost. As a compromise, we calculate the average normalized MGHs fixing $z_{\text{lim}}=0.08$, which corresponds to $t_{\text{lb}} \approx 1.0$ Gyr for the cosmology used here. The MGHs of galaxies observed at lower redshifts are interpolated and renormalized to start at $z = 0.08$.

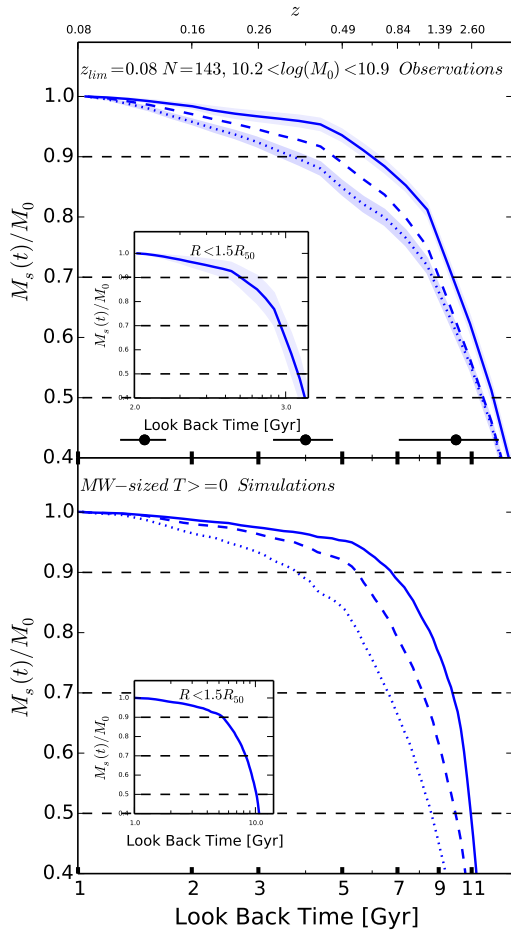


Figure 10. Normalized archaeological global and radial MGHs of disk/lenticular MW-sized galaxies from observations (upper panel) and simulations (lower panel). The global MGHs were calculated inside 1.5 effective radii, and the radial MGHs were calculated within radial bins corresponding to 0–0.5, 0.5–1, and 1–1.5 R_{eff} ; solid, dashed, and dotted lines, respectively. For the observations, MW-sized galaxies of morphological type $T \geq 0$ and $i < 75$ degree from the MaNGA/SDSS-IV sample (MPL-5 data reduction pipeline) were used. The shaded areas are the errors of the mean. The horizontal error bars are estimates of the methodological uncertainty in the determination of the stellar population ages at three look-back times. For the simulations, the disk-dominated + lenticular-like galaxies were used.

The upper panels of figures 10 and 11 show the average global and radial normalized MGHs of the MW-sized MaNGA subsamples of spiral/lenticular ($T \geq 0$) and blue/star-forming early-type ($T < 0$) galaxies, respectively, from $t_{\text{lb}} = 1$ Gyr. The shaded areas indicate the error of the mean for the global (inside 1.5 R_{eff} ; inset) and for the innermost and outermost radial MGHs (solid and dotted lines, respectively). The radial MGHs correspond to the average in three radial bins: (0, 0.5), (0.5, 1) and (1, 1.5) R_{eff} , where R_{eff} is the effective radius of the galaxies in the r band. The horizontal error bars give an estimate of the methodological uncertainty in the determination of the stellar population ages; the observed spectra poorly constrain the ages of the oldest stellar populations. The lower panels of figures 10 and 11 show the corresponding average and radial normalized MGHs of our simulations, for which we use the archaeological radial MGHs (see subsection 3.2). The global MGHs (insets) are calculated within 1.5 $R_{0.5}$. The half-mass radius, $R_{0.5}$, is typically smaller than the r band effective radius, R_{eff} , but the differences are small (on average 25% in the g band and less in the r band, Szomoru et al. 2013), so that the averages calculated in wide radial bins normalized to one or another radius are very similar.

According to the insets of figure 10, the average global archaeological MGH of $T \geq 0$ MW-sized galaxies from observations is slightly shifted at small mass fraction to larger look-back times with respect to the results from our simulations. The look-back times at which 50% and 70% of the final stellar masses are attained are on average 1.90 and 0.97 Gyr older for the observed galaxies than for the simulated ones, respectively; for the 90% of the final mass, the average trend changes and the observed galaxies assembled 0.32 Gyr later than the observed ones. As discussed in subsection 5.3 of Ibarra-Medel et al. (2016, see also Leitner 2012), the statistical and systematic uncertainties in the fossil record method seem to work in the direction of biasing the early mass assembly inferences to earlier epochs, and the late assembly to slightly later epochs.

The radial MGHs of the $T \geq 0$ galaxies show a clear inside-out trend, both for the fossil record inferences (see also Ibarra-Medel et al. 2016) and the simulations. However, in more detail, *the simulations show a more pronounced inside-out trend than the observational inferences*. While the innermost normalized MGHs are quite similar, the intermediate and outermost radial bins from the simulations assemble on average later than those inferred from observations. This difference can be partially accounted for the fact that most of galaxies are observed with some inclination with respect to the face-

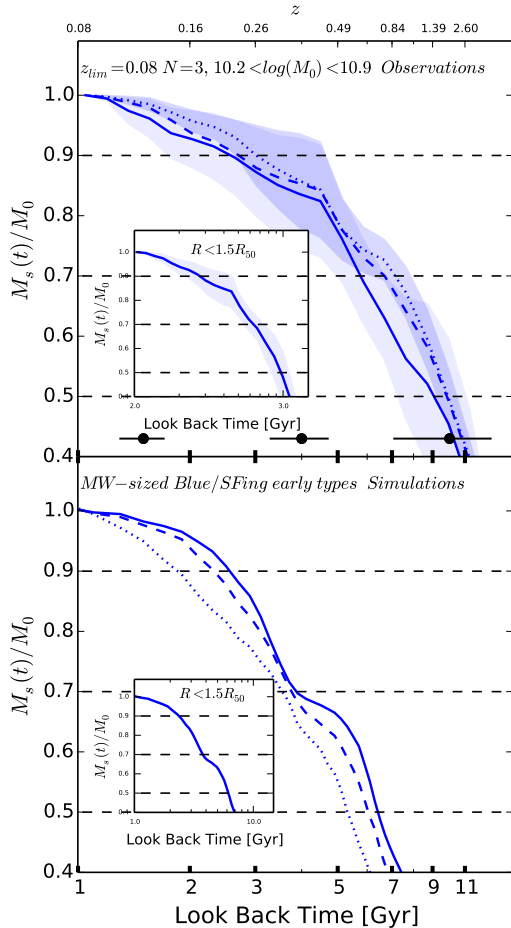


Figure 11. As in figure 10 but for MaNGA blue/star-forming early-type MW-sized galaxies (upper panel) and the Sp4S/Sp5S simulated galaxies (lower panel).

on position. For an inclined galaxy, the stellar populations along the line of sight of a given radial stellar bin are contaminated by the stellar populations of the other radial bins. As the result, the inferred radial MGHs tend to homogenize among them, the more as the inclination is larger. However, mock observations of some of our galaxies show that this effect becomes important only for inclinations larger than ~ 70 degrees (Ibarra-Medel et al. 2017, in prep.).

Regarding the rare blue, star-forming early-type galaxies in the $M_s = 2 - 8 \times 10^{10} M_\odot$ range, there are only three in the MaNGA current sample. The average normalized global MGH for them (inset in figure 11) reveals a late formation/assembly of their stellar populations (70% of its mass formed at $t_{\text{lb}} \sim 6.3$ Gyr). The simulated galaxies of this type also have a late stellar mass formation/assembly due to the late major mergers that they suffer, with 70% of the mass formed

on average at $t_{\text{lb}} \sim 4$ Gyr. For the 90% of the assembled mass, $t_{\text{lb}} = 2.7$ and 2.4 Gyr for the average of the observations and simulations, respectively. The radial normalized MGHs, both for observations and simulations, are much closer among them than in the case of the $T \geq 0$ galaxies. The effects of mixing stellar populations of different galaxies during the mergers as well as merger-induced radial flows work in the direction of producing a nearly homogeneous radial distribution of stellar populations. The observational inferences seem to suggest even an outside-in formation, however, the error of the mean around each radial MGH is large. Looking individually each one of the three blue, star-forming early-type galaxies, two of them show periods of both inside-out and outside-in formation modes. We can conclude that at a qualitative level some observed blue, star-forming early-type galaxies can be explained as the product of late major mergers of disk galaxies, though the rejuvenation scenario (early formation, as most of normal early-type galaxies, but late gas infall that triggers SF specially in the central regions) is also possible (see subsection 6.2).

5.2. Inferences from look-back time observations

In van Dokkum et al. (2013), results of the inner and outer mass assembly of progenitors of MW-sized galaxies since $z \sim 2.5$ were presented. These authors have used the technique of linking progenitor and descendant galaxies by requiring that they have the same (cumulative) comoving number density (see e.g., Brown et al. 2007; van Dokkum et al. 2010). The descendant galaxies at $z \sim 0$ are chosen to have stellar masses around $5 \times 10^{10} M_\odot$ and for the selected progenitors, stacked images at different redshifts from the 3D-HST and CANDELS Treasury surveys are used. From the stacked mass surface density profiles of the progenitors, the evolution of the stellar mass contained inside and outside 2 kpc (physical scale), as well as the total mass, is presented.

Figure 12 shows the average current MGHs inside and outside 2 kpc and the total MGHs, as in figure 4 of van Dokkum et al. (2013) (red, blue, and black lines, respectively). For the averages and standard deviations, we have used all the simulations but Sp4S and Sp5S since they correspond to very peculiar cases. Simulations and observational inferences show the same trends: at high redshifts the mass within the inner 2 kpc grows with time slightly slower than the mass outer than 2 kpc, and at lower redshifts the difference between both rates increases to the point that the inner mass stops growing while the outer mass continues growing. In more detail, however, the simulations show an earlier total mass assembly and a larger difference between the in-

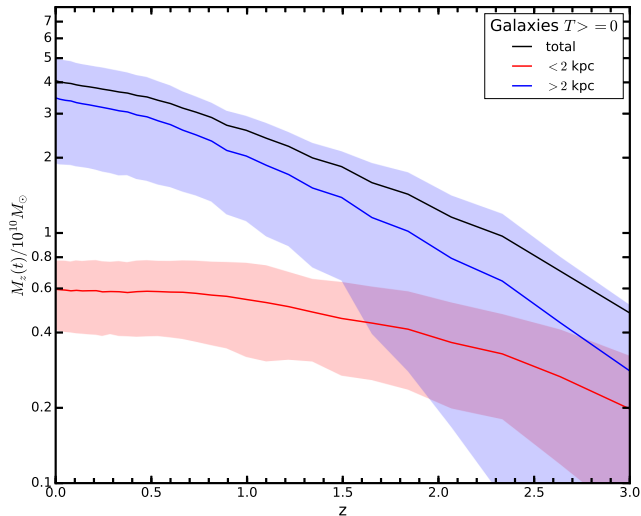


Figure 12. Average global, inner, and outer current stellar MGHs from the disk-dominated + lenticular-like simulated galaxies (late-type like, $T \geq 0$). Black line is for the total stellar mass, while red and blue lines are for the stellar mass inside and outside 2 kpc, respectively. The shaded areas show the standard deviations. This plot should be compared to the observational inferences by [van Dokkum et al. \(2013\)](#) (their figure 4). The outer regions grow on average much faster than the inner ones. The latter ones almost stop growing since $z \sim 1$; the SF quenches within the innermost 2 kpc.

ner and outer mass growth rates since $z \sim 1$ than the empirical inferences. The strong slowdown of the inner mass growth starts at higher redshifts in the simulations ($z \sim 1$ on average) than in the empirical inferences ($z \sim 0.6$). Note that the inner SF quenching in our simulations happens efficiently since high redshifts (see also Section 4), in spite of we are not including the effects of AGN feedback.

Summarizing, *our simulations show a more pronounced inside-out stellar mass growth than the empirical inferences by van Dokkum et al. (2013) show.*

5.3. Half-mass radius evolution

The empirical size evolution of MW-sized galaxies has been obtained by some authors by selecting the observed main progenitors at different redshifts under the requirement that they have the same (cumulative) comoving number density at all redshifts ([van Dokkum et al. 2013](#)) or by using the stellar mass growth inferred from the evolution of the star-forming sequence ([Patel et al. 2013](#)) or from abundance-matching techniques ([Papovich et al. 2015](#)). In Figure 13 we present the median half-mass radius evolution of our galaxies (excluding runs Sp4S and Sp5S), as well as the percentiles corresponding to a 1σ deviation, and compare them with those obtained by

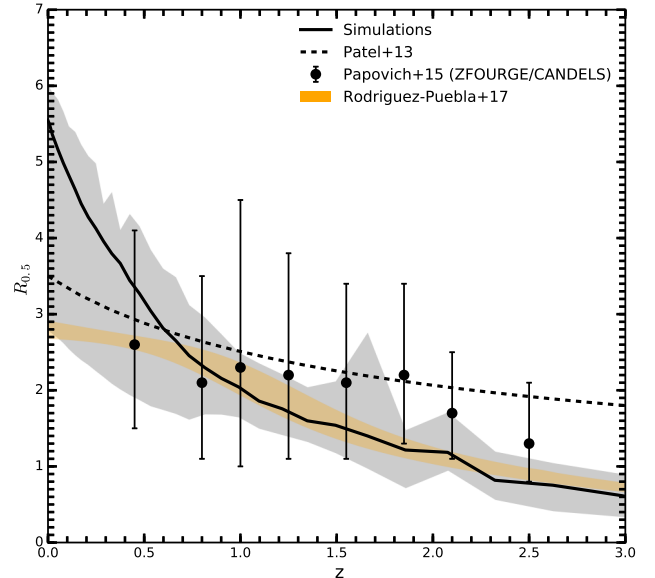


Figure 13. Median values of $R_{0.5}$ as a function of z for the simulations (excluding runs Sp4S and Sp5S; solid line) and the percentiles corresponding to a $1\text{-}\sigma$ deviation (shaded area). The corresponding estimates from look-back observational studies of MW-sized progenitors by [Papovich et al. \(2015\)](#) and [Patel et al. \(2013\)](#) are also plotted. The latter authors report only the best fit to their results. We also plot the results from the semi-empirical approach by [Rodríguez-Puebla et al. \(2017\)](#), for galaxies of present-day stellar masses between $2\times$ and $8 \times 10^{10} M_{\odot}$.

[Papovich et al. \(2015, dots with error bars\)](#) and [Patel et al. \(2013, dot-dashed line for their fit to the data\)](#). We also plot the semi-empirical inferences from [Rodríguez-Puebla et al. \(2017\)](#) for galaxies in halos with present-day masses between $0.8\times$ and $1.6 \times 10^{12} M_{\odot}$, corresponding to stellar masses between $2\times$ and $8 \times 10^{10} M_{\odot}$ (the orange shaded area encompasses this range of masses). These authors, under some assumptions and using the observational constraints on the size–mass relation of star-forming and quiescent galaxies at different redshifts, have extended the semi-empirical approach (e.g., [Behroozi, Wechsler & Conroy 2013](#)) for constraining the radial stellar mass distribution of the evolving galaxies, assumed as disk-bulge systems with disk and bulge mass fractions proportional to the fractions of star-forming and quiescent galaxies, respectively.

As seen in Figure 13, the galaxy size increases as z is lower both in simulations and in the empirical or semi-empirical inferences of MW-sized galaxies *but this growth is stronger in the former than in the latter*. This can be also seen from the evolutionary relation between $R_{0.5}(z)$ and $M_s(z)$. According to [van Dokkum et al. \(2013\)](#), $R_{0.5}(z) \propto M_s(z)^{\alpha}$, with $\alpha = 0.27$ on average up to $z \sim 2.5$ (the average slope is even shallower for the

observations by Papovich et al. 2015). For our simulations, very roughly $\alpha \sim 1$ at $z < 1$ (the slope becomes flatter as z is higher), i.e., the effective radius of the simulated galaxies grows with mass faster than the observational inferences of van Dokkum et al. (2013) and Papovich et al. (2015).

For only the disk-dominated simulations and at $z \sim 0$, the median (mean) value of α is 0.5 (0.7). That is, the growth in size is on average ~ 0.5 times the rate at which they grow in mass. This is larger than the value of $\alpha \sim 0.35$ determined by Pezzulli et al. (2015) from combining empirical scaling relations of disk galaxies and assuming they do not evolve. These authors have tested that this value is consistent with observational determinations for a sample of late-type local galaxies using their stellar and SFR surface density profiles.

The strong $R_{0.5}$ growth of the simulated galaxies evidences a pronounced inside-out structural growth and/or the effect of inside-out quenching of the SF. The latter is probably happening more efficiently in our simulations than in the observed galaxies.

6. DISCUSSION

6.1. Inside-out growth and inside-out quenching

The rate at which increases the half-mass radius of our ‘field’ MW-sized galaxies is on average faster than current observational inferences and simple predictions of disk galaxy evolution in growing CDM halos (see figures 13 and 1, respectively). These predictions are under the assumption of detailed angular momentum conservation and refer to the structural mass growth of the disks driven by the cosmological growth of the halos. For example, at $z = 1$, for all the simulations but Sp2L, $R_{0.5}(z=1) = 0.3 \div 0.5 R_{0.5}(z=0)$, while for the models by Firmani & Avila-Reese (2009, see also e.g., Somerville 2009), $R_{0.5}(z=1) \gtrsim 0.5 R_{0.5}(z=0)$. In the same way, the normalized radial current MGHs of our galaxies, specially the disk-dominated ones, show a more pronounced inside-out stellar mass assembly than observational inferences (figures 10 and 12). Following, we discuss on two physical processes present in the simulations that work in the direction of amplifying the original structural inside-out growth of disks.

Positive stellar feedback.- The adequate modeling of this feedback is a key ingredient to avoid the angular momentum catastrophe problem and to form realistically looking MW-sized disk galaxies (see e.g., Scannapieco et al. 2008; Agertz, Teyssier & Moore 2011; Guedes et al. 2011; Aumer et al. 2013; Stinson et al. 2013; Marinacci, Pakmor & Springel 2014; Übler et al. 2014; Roca-Fàbrega et al. 2016; Colín et al. 2016; Ma et al. 2017; Grand et al. 2017). The feedback drives

an efficient redistribution of the angular momentum of the baryons, which promotes the formation of extended disks, where stars form mostly in-situ out of the disk gas. At a global level, the early conversion of low angular momentum gas into stars is lowered, making the SF histories flatter, with less SF at high redshifts and more SF at low redshifts (Übler et al. 2014). A key feature of our simulated galaxies is that most of the stars are formed indeed in situ, and their SF histories are not strongly peaked at early epochs, showing even significant SF at late times (see also Grand et al. 2017). As shown in Übler et al. (2014), a fraction of the low-angular momentum ejected gas is re-accreted later (galactic fountain), but some of this re-accreted gas attains higher specific angular momentum, eventually through mixing with the hot corona gas or from cosmic torques, and it infalls at larger radii. This process works in favor of strengthen the inside-out growth of the simulated galaxies. As the result of the stellar-driven feedback, as shown in Übler et al. (2014), the specific angular momentum of the stars formed mostly in-situ out of the disk gas, becomes comparable or even higher than the one of the halo. The specific angular momentum of our disk-dominated galaxies grows significantly with time, specially at late epochs (see Colín et al. 2016). As in Übler et al. (2014), we find that the $z \sim 0$ average specific angular momentum of our disk-dominated galaxies is similar or larger than the one measured in their corresponding dark matter halos.

Inside-out SF quenching.- This is the second process that works in the direction of increasing the relative inside-out growth mode of galaxies. The rate of mass growth due to SF suddenly changes from very fast to very slow in the innermost regions, while this rate changes much more gradually in the outer regions (excepting for the Sp2L galaxy; figure 3). Indeed, the inner regions (e.g., < 1 kpc) have typically much earlier SF histories than all the galaxy (figure 6). The inner gas-to-stellar mass ratios, $M_{g,cold}/M_s = t_{\text{depl}}/t_{\text{sf}}$, decrease to very low values since $z \sim 4 - 2$ (figure 7). These values become much smaller than 0.1, suggesting that the central regions of the simulated galaxies enter into a long-term quenching phase very soon. Instead, the $t_{\text{depl}}/t_{\text{sf}}$ ratios of the whole galaxy do not decrease to values much smaller than 0.1. The metabolism of the inner regions of the simulated galaxies is very different to the metabolism of the outer regions.

The inside-out quenching seen in our MW-sized simulations, specially the disk dominated ones, strengthens the structural inside-out trend of the stellar mass assembly. We highlight that this inside-out quenching process is without the presence of an AGN, and it is produced mainly by a burst of SF in the early compact galaxy, the

consequent depletion of a high fraction of gas, the expulsion by SN-driven feedback of another fraction, and the absence of mechanisms of further significant gas replenishment to the central regions (a qualitatively similar result has been found in numerical simulations at high redshifts by Tacchella et al. 2016b, see also Zolotov et al. 2015, Tacchella et al. 2016a). Once the disks are well established after $z \sim 1$, secular processes could contribute to transport fresh gas (and stars) to the centre, leading this to a more homogeneous radial stellar mass assembly. However, this seems not to be the case in our simulations, at least not at a significant level. One of the main mechanisms of angular momentum and mass transport within the disk is the bar. In most of our simulations bars are actually not formed efficiently (in a forthcoming paper, a detailed analysis on bar formation/destruction will be presented).

Other mechanisms.- Grand et al. (2017) show that SF in their MW-sized simulations, as in our case, happens mostly in-situ, and with a radial distribution that may be categorized into either centrally concentrated or radially extended, inside-out formation. For the simulations that end with large disk scalelengths, they find that gas-rich quiescent mergers work as a mechanism by which the halo dark matter and gas acquire a high degree of specific angular momentum, which leads to high-angular momentum star-forming material condensing around the disk, and therefore to enhanced inside-out SF and large discs. We will explore whether this mechanism is also relevant or not in our simulations elsewhere. Grand et al. (2017), who included AGN feedback in their simulations, show also that the effect of this feedback is mild in terms of the disk size. The most important effect of AGN feedback is to suppress central SF. This suppression prevents the formation of overly massive bulges in galaxies with high gas densities in the centre.

Finally, we note that the relatively fast evolution of the innermost galaxy regions in our simulations (early and strong SF peak and a consequent long-term quenching; figure 6) implies that the simulated galaxies were too compact at high redshifts ($z > 2-3$). The half-mass radii at these redshifts are indeed small (figure 13). A similar result has been reported by Jung, Cen & Bryan (2009), who claim that any potential viable solution to this apparent problem would have to reduce the amount of stars that are formed at very early epochs. The authors suggest as possible mechanisms: (1) an early reionization with $z_{\text{ri}} \gg 6$, a strong, internal stellar- or AGN-driven feedback, or (3) a small-scale cut-off in the matter power spectrum, for instance if the dark matter is warm rather than cold.

6.2. *The blue, star forming early-type galaxies*

In our suite of eight “field” MW-sized galaxies, two suffered late major mergers, making these galaxies to be spheroid dominated but yet blue and star forming at $z = 0$. In the local Universe these kind of galaxies are rare but they exist in isolated environments (e.g., Lacerna et al. 2016, and more references therein). Given the qualitative rough agreement found between the global and radial MGHs of simulated and observed galaxies (subsection 5.1), we could conclude that the rare blue, star-forming early-type galaxies found in the local Universe can be explained as the result of late major mergers. However, there is room also for the mechanism of rejuvenation. In this case, the blue, star-forming galaxy forms similarly to other early-type galaxies but lately suffers gas accretion, and the SF activates, specially in the center (see for a discussion Lacerna et al. 2016). In our small set of simulations, we do not have this case.

7. SUMMARY AND CONCLUSIONS

We have studied the global and radial stellar mass growth histories, MGHs, of ‘field’ MW-sized galaxies simulated with the N-body + Hydrodynamics ART code and presented previously in Colín et al. (2016). From our suite of eight simulations (see Table 2), four are disk dominated at $z = 0$ (D) two are lenticular like (L), and two are largely dominated by the spheroid but are blue and star-forming at $z = 0$ (S; they suffered recent major mergers). Our main results and conclusions are as follow:

(i) The stellar half-mass radius, $R_{0.5}$, increases with cosmic time, with some periods of shrinkage only at very early times or when late major mergers happened in the case of runs Sp4S and Sp5S. The late growth of $R_{0.5}$ is very fast in all the runs, actually, faster than predictions of formation of disks in centrifugal equilibrium from baryons that conserve the angular momentum distribution of their growing Λ CDM host halos (figure 1).

(ii) The radial current normalized MGHs evidence an inside-out stellar mass growth, which is more pronounced in the disk-dominated galaxies and less pronounced in the late-merging spheroid-dominated ones or even inverse at some epochs in the lenticular-like Sp2L galaxy (figure 2). Since the current MGHs take into account gain/loss of stellar particles in/from the given radial bin as well as the stellar mass loss by winds, the radial MGHs some times can decrease. This happens specially when the galaxy suffers mergers. The in-situ radial normalized MGHs (accounted for only stellar particles formed in the given radial bin and “frozen” there, taking into account the mass loss by stellar winds) follow closely the respective current radial MGHs (figure

3). This and other pieces of evidence show that (1) the radial stellar mass assembly of the simulated galaxies is driven by in-situ SF (the dynamical assembly due to mergers does not change significantly the inside-out growth mode), and (2) galaxies do not suffer a significant net radial stellar mass transport in such a way that the established radial stellar mass distribution does not change dramatically.

(iii) For the representative runs Sp8D and Sp6L, we have measured the radial displacement each stellar particle suffered. On average, indeed the particles do not show a net radial transport though they may shift in both radial directions by ≈ 1.8 and 0.9 kpc at the $1\text{-}\sigma$ level, respectively. We caution that due to the spatial resolution limit in our simulations (the cell length at the greatest level of refinement is $109h^{-1}$ pc), dynamical processes associated to radial migration are likely underestimated.

(iv) The in-situ radial MGHs of all runs evidence an early fast growth by SF in the innermost radial bin followed by an abrupt slowdown, to the point that the innermost radial bin stops growing. The outer radial bins follow qualitatively this trend but much more gradual as more external they are. Within the inner 1 kpc, the sSFR decreases with cosmic time faster and the depletion time becomes much shorter than in all the galaxy, specially for the disk-dominated simulations. As the result, the $t_{\text{depl}}/t_{\text{sf}}$ ratios (equal to the gas-to-stellar mass ratios) inside 1 kpc decrease much more abruptly than for all the galaxy. These ratios inside 1 kpc become $\ll 0.1$, showing that the inner regions entered into a long-term quenching phase, while for the whole galaxy, these ratios remain above ~ 0.1 . Therefore, our galaxies quench their SF the inside out, and as a consequence the mass growth by in-situ SF slows down more efficiently in the inner regions than in the outer ones. The exception is run Sp2L (see above); this early-assembling lenticular-like galaxy is the one with the most homogenous radial MGHs and highest gas fraction among all the runs.

(v) The global and radial archaeological MGHs (constructed from the $z = 0$ stellar particle age distributions) are similar to the current ones, showing this again that neither the mergers nor the radial net mass transport play a significant role in the structural evolution of our MW-sized galaxies. The exception is during the periods of major mergers. When galaxies suffered late major mergers, the archaeologically inferred MGHs are shifted to earlier epochs with respect to the current MGHs.

(vi) We have compared our archaeological MGHs with those inferred by means of the fossil record method applied to the MaNGA survey (Ibarra-Medel et al. 2016) in the same M_s range as our simulations. For the spi-

ral/lenticular ($T \geq 0$) subsample, the predicted and observationally inferred MGHs are in qualitative agreement, both evidencing the inside-out trend (figure 10). However, the observational inferences show a less pronounced inside-out trend than the simulations. For the rare blue, star-forming early-type galaxies (only two in our simulations and three in the observations), the MGHs are significantly later than those of the other galaxies, and qualitatively agree between simulations and observations (figure 11).

(vii) The average mass growth histories inside an outside 2 kpc agree qualitatively with empirical inferences from look-back observations of MW-sized galaxy progenitors (van Dokkum et al. 2013): the outer regions grow faster than the inner ones (figure 12). However, this inside-out mode is more pronounced in the simulations than in the observations. The half-mass radius of the simulated galaxies also grows faster on average than estimates from look-back observations of the progenitors of MW-sized galaxies (van Dokkum et al. 2013; Patel et al. 2013; Papovich et al. 2015).

Since at MW-size scales the (uncertain) effects of stellar and AGN feedback are less critical for galaxy evolution than at other scales, it is likely that our simulations do not differ substantially with respect to other recent simulations of MW-sized galaxies in spite of the differences in the feedback implementations. In this sense, we believe that the results presented here regarding the global and radial stellar mass assembly of MW-sized galaxies formed in the Λ CDM scenario are generic, regardless of numerical details and feedback prescriptions. Our main finding is that these galaxies assemble their masses the inside out, driven mainly by in-situ SF and by an inside-out process of SF quenching. The latter happens without the presence of an AGN, in agreement with results found by Tacchella et al. (2016b) for high-redshift simulations.

Qualitatively, our results are consistent with current observational inferences of the global and radial stellar mass growth from the fossil record method and from look-back time observations. However, in more detail, *the simulations predict a more pronounced inside-out mode and a faster half-mass radius growth than all these observational inferences*. As discussed in Section 6, besides the structural inside-out mass build up, the simulated galaxies suffer also of some gas redistribution due to the SN-driven feedback (fountain effect) and of inside-out slowdown/quenching of SF (excepting Sp2L). Both effects tend to strengthen the inside-out mode and the rate of $R_{0.5}$ growth. Are these effects too efficient in our simulations? Recall that we even did not include the effect of AGN-driven feedback, which is expected to

enhance the inside-out quenching of SF. Do other simulations of MW-sized galaxies, where different schemes of SF and feedback were implemented, face the same potential problems of too pronounced inside-out growth mode and half-mass radius growth? It is of great interest in the field to provide answers to these questions. So far, current numerical simulations and observational inferences start to be able to constrain not only the evolution of the global properties of galaxies but also the local ones.

We thank an anonymous referee for useful comments and suggestions, which improved the quality of the manuscript. A.G-S. was financially supported by a UC-MEXUS Fellowship. H.I-M. was financially supported by a postdoctoral fellowship provided by CONACyT grant (Ciencia Básica) 180125. This paper is dedicated to the memory of our friend and colleague Pedro Colín, who sadly passed away on January 14th 2017.

APPENDIX

A. CUMULATIVE STELLAR MASS DISTRIBUTIONS

A way to evaluate how much the radial stellar mass distribution of the galaxies has changed by net radial mass flows and/or mergers is by comparing the $z = 0$ current cumulative radial stellar mass distribution, $M_s(< R)$, with the cumulative radial distribution of the stellar particles formed in-situ at each radial bin and frozen there, i.e., not taking into account the possible displacement of stellar particles from the given radial bin or particles that come from outside this bin (the stellar mass loss of the accumulated in-situ stars in the bin is taken into account), see also [El-Badry et al. \(2016\)](#). Such a comparison is shown in figure 14 for the eight simulated galaxies: black solid line is for the current radial mass distribution and black dotted line for the hypothetical in-situ SF radial mass distribution. In general, both distributions are very similar, showing that *the stellar particles formed in-situ did not suffer significant net radial re-distribution and that mergers do not alter too much the global radial stellar mass distribution*. In four cases the inner current cumulative radial mass distribution is slightly more concentrated than the one corresponding to the in-situ born stellar particles (the highest difference is for the Sp2L galaxy). This could be due to some external stellar mass incorporated into the inner regions (mergers), due to some inward stellar mass transport or due to outside-in SF quenching. In Section B we show that most of the radial stellar displacements are more radial mixing at relatively small scales than net inward or outward transport.

In figure 14 are also shown the in-situ cumulative stellar mass profiles at redshifts higher than $z = 0$ (color dotted lines). The evolution of the cumulative radial mass distribution of in-situ born stellar particles shows a clear inside-out growth in all the cases but the Sp2L galaxy (since $z \sim 1.5$). For the Sp2L galaxy, since $z \sim 1.5$ to ~ 0.5 , the in-situ radial cumulative stellar mass distribution becomes slightly more compact. This is because the SFR slows down progressively from the outermost regions to the inner ones (see Section 4).

B. RADIAL DISPLACEMENTS OF THE STELLAR PARTICLES

The comparison between the current and in-situ radial MGHs presented in Section 3 and the comparison between the $z = 0$ cumulative stellar mass profiles of all the stellar particles and those that formed only in-situ (figure 14) strongly suggest that our simulated galaxies do not suffer significant radial mass redistributions by dynamical processes. Here, we measure directly the radial displacement of each stellar particle between its final position (at $z = 0$) and its position at birth, $t_{\text{lb, birth}}$ for two representative runs, Sp8D and Sp6L. In figure 15 we present the results of this analysis, where the mean and standard deviation (solid line and shaded area) of the radial displacements in small bins of $t_{\text{lb, birth}}$ are plotted. We also plot in these figures the half-mass radius at each time both in the positive and negative side of the displacement (red line) with the aim to compare the radial shifts with the characteristic scales of the galaxy.

The disk-dominated Sp8D galaxy presents a stellar MGH extended to late times and it is the one with the most pronounced inside-out growth (see figure 2). Figure 15 shows that the stellar particles on average remain close to the radial positions where they were born, that is, there are not significant net radial mass flows. If any, there is a mild trend for the youngest particles, born mainly in the outermost regions, to shift inwards on average by ~ 0.5 kpc (see also the pink line in figure 2). This shift is very small compared to the characteristic scales of the galaxy at $z \sim 0$. In general, the stellar particles scatter similarly inward and outward with respect to their birth radius by no more than ≈ 1.8 kpc at the $1-\sigma$ level. This kind of radial mixing is more pronounced for the particles older than ~ 8 Gyr; the $1-\sigma$ shifts are actually larger than the characteristic scales of the galaxy at the epochs these particles were born. Along with the net inward mass transport, there is also an increase in the radial mixing scales for the particles younger

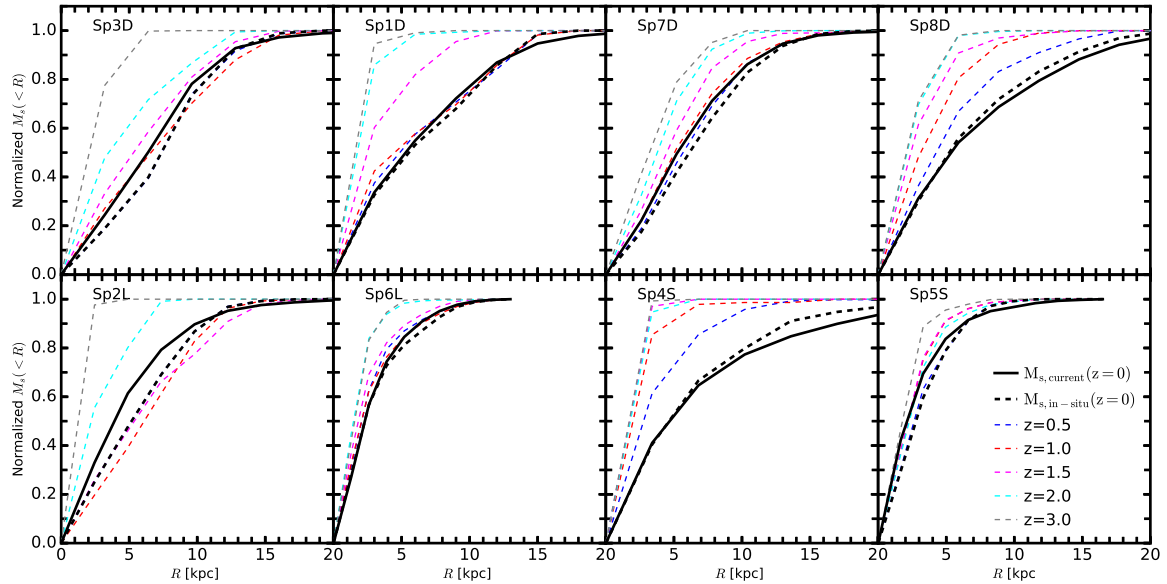


Figure 14. Cumulative stellar mass radial distribution, $M_s(< R)$, of the simulated galaxies at $z = 0$ (solid lines). The black dashed lines are the cumulative radial distributions of the stellar particles formed in-situ at each radius and frozen there until $z = 0$ (the stellar mass loss by winds is taken into account). If mergers and radial mass transport are not relevant in the structural mass assembly of the galaxy, then both cumulative radial distributions are expected to be similar. The in-situ frozen cumulative radial distributions are also shown at different redshifts (color lines; see the color code in the inset). A clear inside-out growth of the stellar disks by in-situ SF is seen.

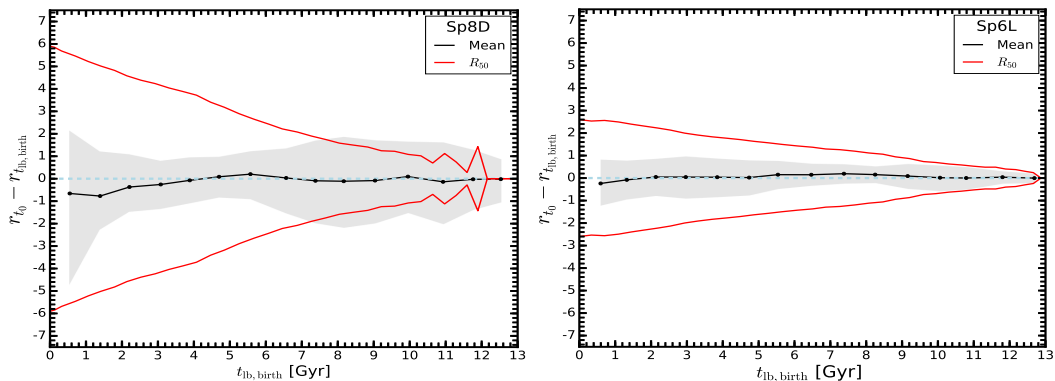


Figure 15. Mean and standard deviation of the radial displacements suffered by the stellar particles since their birth at a given look-back time and the present-day time for the runs Sp8D and Sp6L. The red line is the half-mass radius at each time both in the positive and negative side of the displacement.

than ~ 2 Gyr, which are mostly the outermost particles. This could be related to the same dynamical process that produces warps in this simulation.

The lenticular-like Sp6L galaxy presents an early stellar mass assembly, without mergers since early epochs and following an inside-out growth mode (see figure 2). Figure 15 shows that the stellar particles on average remain close to the radial positions where they were born, that is, again there are not significant net radial mass flows. The stellar particles scatter similarly inward and outward with respect to their birth radius by no more than ≈ 0.9 kpc at the $1\text{-}\sigma$ level. These displacements are much smaller than the characteristic size of the galaxy since ~ 9 Gyr ago.

We should stress that the results presented above are very general. A more detailed analysis, taking into account the stellar particle orbits, is necessary to study the question of stellar migration from the point of view of galactic dynamics. For this kind of studies, a higher spatial resolution than in our simulations is likely required. However, our numerical results seem to be in line with a radial mixing process happening in isolated MW-sized galaxies rather than

a net radial migration able to change significantly the stellar surface density profile (e.g., Schönrich & Binney 2009; Roškar et al. 2012).

REFERENCES

- Abolfathi B. et al., 2017, ArXiv e-prints
- Agertz O., Teyssier R., Moore B., 2011, MNRAS, 410, 1391
- Athanassoula E., 2003, MNRAS, 341, 1179
- Aumer M., White S. D. M., Naab T., 2014, MNRAS, 441, 3679
- Aumer M., White S. D. M., Naab T., Scannapieco C., 2013, MNRAS, 434, 3142
- Avila-Reese V., Colín P., González-Samaniego A., Valenzuela O., Firmani C., Velázquez H., Ceverino D., 2011, ApJ, 736, 134
- Avila-Reese V., Firmani C., 2000, RMxAA, 36, 23
- Avila-Reese V., Firmani C., Hernández X., 1998, ApJ, 505, 37
- Barnes J. E., Hernquist L., 1996, ApJ, 471, 115
- Behroozi P. S., Wechsler R. H., Conroy C., 2013, ApJ, 770, 57
- Berrier J. C., Sellwood J. A., 2016, ApJ, 831, 65
- Bilitewski T., Schönrich R., 2012, MNRAS, 426, 2266
- Bird J. C., Kazantzidis S., Weinberg D. H., Guedes J., Callegari S., Mayer L., Madau P., 2013, ApJ, 773, 43
- Boeche C. et al., 2014, A&A, 568, A71
- Boissier S., Prantzos N., 2000, MNRAS, 312, 398
- Bouwens R., Silk J., 2002, ApJ, 568, 522
- Brooks A., Christensen C., 2016, Galactic Bulges, 418, 317
- Brown M. J. I., Dey A., Jannuzi B. T., Brand K., Benson A. J., Brodwin M., Croton D. J., Eisenhardt P. R., 2007, ApJ, 654, 858
- Bundy K. et al., 2015, ApJ, 798, 7
- Chabrier G., 2003, PASP, 115, 763
- Cheng J. Y. et al., 2012, ApJ, 746, 149
- Colín P., Avila-Reese V., Roca-Fàbrega S., Valenzuela O., 2016, ApJ, 829, 98
- Dale D. A. et al., 2016, AJ, 151, 4
- Dalla Vecchia C., Schaye J., 2012, MNRAS, 426, 140
- Debattista V. P., Mayer L., Carollo C. M., Moore B., Wadsley J., Quinn T., 2006, ApJ, 645, 209
- Dekel A., Birnboim Y., 2006, MNRAS, 368, 2
- Dekel A., Burkert A., 2014, MNRAS, 438, 1870
- Di Teodoro E. M., Fraternali F., 2014, A&A, 567, A68
- Dobbs C. L., Pringle J. E., Burkert A., 2012, MNRAS, 425, 2157
- Dobbs C. L., Pringle J. E., Duarte-Cabral A., 2015, MNRAS, 446, 3608
- Dutton A. A., 2009, MNRAS, 396, 121
- El-Badry K., Wetzel A., Geha M., Hopkins P. F., Kereš D., Chan T. K., Faucher-Giguère C.-A., 2016, ApJ, 820, 131
- Elmegreen B. G., Bournaud F., Elmegreen D. M., 2008, ApJ, 688, 67
- Faber S. M. et al., 2007, ApJ, 665, 265
- Fall S. M., Efstathiou G., 1980, MNRAS, 193, 189
- Faucher-Giguère C.-A., Kereš D., Ma C.-P., 2011, MNRAS, 417, 2982
- Ferland G. J., Korista K. T., Verner D. A., Ferguson J. W., Kingdon J. B., Verner E. M., 1998, PASP, 110, 761
- Firmani C., Avila-Reese V., 2000, MNRAS, 315, 457
- Firmani C., Avila-Reese V., 2009, MNRAS, 396, 1675
- García-Benito R. et al., 2017, A&A, 608, A27
- Goddard D. et al., 2017, MNRAS, 466, 4731
- González Delgado R. M. et al., 2016, A&A, 590, A44
- Grand R. J. J. et al., 2017, MNRAS, 467, 179
- Guedes J., Callegari S., Madau P., Mayer L., 2011, ApJ, 742, 76
- Gunn J. E., 1982, in Astrophysical Cosmology Proceedings, Brueck H. A., Coyne G. V., Longair M. S., eds., pp. 233–259
- Haardt F., Madau P., 1996, ApJ, 461, 20
- Hayden M. R. et al., 2014, AJ, 147, 116
- Ibarra-Medel H. J. et al., 2016, MNRAS, 463, 2799
- Joung M. R., Cen R., Bryan G. L., 2009, ApJL, 692, L1
- Kennedy R., Bamford S. P., Häußler B., Brough S., Holwerda B., Hopkins A. M., Vika M., Vulcani B., 2016, A&A, 593, A84
- Klypin A., Holtzman J., 1997, ArXiv Astrophysics e-prints
- Kormendy J., 2016, Galactic Bulges, 418, 431
- Kravtsov A. V., 2003, ApJL, 590, L1
- Kravtsov A. V., Klypin A. A., Khokhlov A. M., 1997, ApJS, 111, 73
- Kravtsov A. V., Nagai D., Vikhlinin A. A., 2005, ApJ, 625, 588
- Lacerna I., Hernández-Toledo H. M., Avila-Reese V., Abonza-Sane J., del Olmo A., 2016, A&A, 588, A79
- Lacerna I., Rodríguez-Puebla A., Avila-Reese V., Hernández-Toledo H. M., 2014, ApJ, 788, 29
- Larson R. B., 1976, MNRAS, 176, 31
- Law D. R. et al., 2016, AJ, 152, 83
- Leitner S. N., 2012, ApJ, 745, 149
- Li C. et al., 2015, ApJ, 804, 125
- Lian J., Yan R., Blanton M., Kong X., 2017, MNRAS, 472, 4679

- Lilly S. J., Carollo C. M., Pipino A., Renzini A., Peng Y., 2013, *ApJ*, 772, 119
- Lin L., Zou H., Kong X., Lin X., Mao Y., Cheng F., Jiang Z., Zhou X., 2013, *ApJ*, 769, 127
- Ma X., Hopkins P. F., Wetzel A. R., Kirby E. N., Anglés-Alcázar D., Faucher-Giguère C.-A., Kereš D., Quataert E., 2017, *MNRAS*, 467, 2430
- Marinacci F., Pakmor R., Springel V., 2014, *MNRAS*, 437, 1750
- Martig M., Bournaud F., Teyssier R., Dekel A., 2009, *ApJ*, 707, 250
- Martin D. C. et al., 2007, *ApJS*, 173, 342
- Mikolaitis Š. et al., 2014, *A&A*, 572, A33
- Miller G. E., Scalo J. M., 1979, *ApJS*, 41, 513
- Mo H., van den Bosch F. C., White S., 2010, *Galaxy Formation and Evolution*
- Mo H. J., Mao S., White S. D. M., 1998, *MNRAS*, 295, 319
- Muñoz-Mateos J. C., Gil de Paz A., Boissier S., Zamorano J., Jarrett T., Gallego J., Madore B. F., 2007, *ApJ*, 658, 1006
- Pan Z., Li J., Lin W., Wang J., Fan L., Kong X., 2015, *ApJL*, 804, L42
- Papovich C. et al., 2015, *ApJ*, 803, 26
- Patel S. G. et al., 2013, *ApJ*, 778, 115
- Peebles P. J. E., 1969, *ApJ*, 155, 393
- Peng Y.-j. et al., 2010, *ApJ*, 721, 193
- Pérez E. et al., 2013, *ApJL*, 764, L1
- Pezzulli G., Fraternali F., 2016, *MNRAS*, 455, 2308
- Pezzulli G., Fraternali F., Boissier S., Muñoz-Mateos J. C., 2015, *MNRAS*, 451, 2324
- Roca-Fàbrega S., Valenzuela O., Colín P., Figueras F., Krongold Y., Velázquez H., Avila-Reese V., Ibarra-Medel H., 2016, *ApJ*, 824, 94
- Rodríguez-Puebla A., Primack J. R., Avila-Reese V., Faber S. M., 2017, *ArXiv e-prints*
- Rodríguez-Puebla A., Primack J. R., Behroozi P., Faber S. M., 2016, *MNRAS*, 455, 2592
- Roškar R., Debattista V. P., Quinn T. R., Stinson G. S., Wadsley J., 2008, *ApJL*, 684, L79
- Roškar R., Debattista V. P., Quinn T. R., Wadsley J., 2012, *MNRAS*, 426, 2089
- Sánchez S. F. et al., 2016a, *RMxAA*, 52, 171
- Sánchez S. F. et al., 2016b, *RMxAA*, 52, 21
- Scannapieco C., Tissera P. B., White S. D. M., Springel V., 2008, *MNRAS*, 389, 1137
- Scannapieco C., White S. D. M., Springel V., Tissera P. B., 2009, *MNRAS*, 396, 696
- Schönrich R., Binney J., 2009, *MNRAS*, 396, 203
- SDSS Collaboration et al., 2016, *ArXiv e-prints*
- Sellwood J. A., Binney J. J., 2002, *MNRAS*, 336, 785
- Sheth K., Vogel S. N., Regan M. W., Thornley M. D., Teuben P. J., 2005, *ApJ*, 632, 217
- Silk J., 1987, in *IAU Symposium, Vol. 124, Observational Cosmology*, Hewitt A., Burbidge G., Fang L. Z., eds., pp. 391–411
- Smethurst R. J., Lintott C. J., Bamford S. P., Hart R. E., Kruk S. J., Masters K. L., Nichol R. C., Simmons B. D., 2017, *MNRAS*, 469, 3670
- Somerville R. S., 2009, *MNRAS*, 399, 1988
- Somerville R. S., Davé R., 2015, *ARA&A*, 53, 51
- Somerville R. S., Hopkins P. F., Cox T. J., Robertson B. E., Hernquist L., 2008, *MNRAS*, 391, 481
- Stinson G., Seth A., Katz N., Wadsley J., Governato F., Quinn T., 2006, *MNRAS*, 373, 1074
- Stinson G. S., Brook C., Macciò A. V., Wadsley J., Quinn T. R., Couchman H. M. P., 2013, *MNRAS*, 428, 129
- Stringer M. J., Benson A. J., 2007, *MNRAS*, 382, 641
- Szomoru D., Franx M., van Dokkum P. G., Trenti M., Illingworth G. D., Labbé I., Oesch P., 2013, *ApJ*, 763, 73
- Tacchella S., Dekel A., Carollo C. M., Ceverino D., DeGraf C., Lapiner S., Mandelker N., Primack J. R., 2016a, *MNRAS*, 458, 242
- Tacchella S., Dekel A., Carollo C. M., Ceverino D., DeGraf C., Lapiner S., Mandelker N., Primack Joel R., 2016b, *MNRAS*, 457, 2790
- Übler H., Naab T., Oser L., Aumer M., Sales L. V., White S. D. M., 2014, *MNRAS*, 443, 2092
- van den Bosch F. C., 2000, *ApJ*, 530, 177
- van den Bosch F. C., 2002, *MNRAS*, 331, 98
- van Dokkum P. G. et al., 2013, *ApJL*, 771, L35
- van Dokkum P. G. et al., 2010, *ApJ*, 709, 1018
- Wang J. et al., 2011, *MNRAS*, 412, 1081
- White S. D. M., 1984, *ApJ*, 286, 38
- White S. D. M., Frenk C. S., 1991, *ApJ*, 379, 52
- White S. D. M., Rees M. J., 1978, *MNRAS*, 183, 341
- Williams B. F., Dalcanton J. J., Dolphin A. E., Holtzman J., Sarajedini A., 2009, *ApJL*, 695, L15
- Zolotov A. et al., 2015, *MNRAS*, 450, 2327